CHARACTERIZATION OF LITHIUM ALUMINUM OXIDE SOLID ELECTROLYTE THIN FILMS FROM AQUEOUS PRECURSORS

by

DONALD R. CLAYTON

A DISSERTATION

Presented to the Department of Chemistry and Biochemistry
and the Graduate School of the University of Oregon
in partial fulfillment of the requirements
for the degree of
Doctor of Philosophy

September 2017

DISSERTATION APPROVAL PAGE

Student: Donald R. Clayton

Title: Characterization of Lithium Aluminum Oxide Solid Electrolyte Thin Films from Aqueous Precursors

This dissertation has been accepted and approved in partial fulfillment of the requirements for the Doctor of Philosophy degree in the Department of Chemistry and Biochemistry by:

Dr. George V. Nazin	Chairperson
Dr. Mark C. Lonergan	Advisor
Dr. Catherine J. Page	Core Member
Dr. Hailin Wang	Institutional Representative

and

Sara D. Hodges	Interim Vice Provost and Dean of the Graduate School

Original approval signatures are on file with the University of Oregon Graduate School.

Degree awarded September 2017

DISSERTATION ABSTRACT

Donald R. Clayton

Doctor of Philosophy

Department of Chemistry and Biochemistry

September 2017

Title: Characterization of Lithium Aluminum Oxide Solid Electrolyte Thin Films from Aqueous Precursors

Low-temperature routes to solid electrolytes are important for construction of solid-state batteries, electrochromic devices, electrolyte-gated transistors, high-energy capacitors and sensors. Here we report an environmentally friendly aqueous solution route to amorphous thin films of solid lithium based electrolytes and related multi-layered structures. This route allows production of high quality films at very low temperatures, up to 600 °C lower than traditional melt quenching routes. Pinhole free films of thicknesses ranging from 13-150 nm produced by this route are extremely smooth and fully dense, with temperature dependent conductivities similar to those reported for samples made by energy intensive techniques. Processing conditions were examined by TGA-DSC; film evolution was monitored by FTIR; and, resulting films were characterized using FTIR, XPS, SEM, and XRD. These techniques indicate that water and nitrate removal is complete at low temperatures, and the films remain amorphous to 400 °C. Electrical analysis suggests the presence of ionic double layer capacitor behaviour as observed in similar metal oxide systems. Large magnitudes of ε'_{app} are reported for two separate systems herein, surpassing values reported in the literature for similar materials produced by other synthetic methods. A two-fold increase in the

breakdown strength of nanolaminate structures over their single-phase counterparts is also reported. The approach developed demonstrates a simple, inexpensive and environmentally benign deposition route for the fabrication of inorganic solid electrolyte thin-films and related nanolaminates, using LiAlPO, LiAlO, and TiO_2:LiAlO as model systems.

This dissertation includes previously published and unpublished co-authored material.

CURRICULUM VITAE

NAME OF AUTHOR: Donald R. Clayton

GRADUATE AND UNDERGRADUATE SCHOOLS ATTENDED:

University of Oregon, Eugene
Central Washington University, Ellensburg

DEGREES AWARDED:

Doctor of Philosophy, Chemistry, 2017, University of Oregon
Master of Science, Chemistry, 2013, University of Oregon
Bachelor of Science, Chemistry, 2010, Central Washington University
Bachelor of Arts, Biology, 2010, Central Washington University

AREAS OF SPECIAL INTEREST:

Materials Chemistry
Inorganic Chemistry
Green Chemistry

PROFESSIONAL EXPERIENCE:

Graduate Research Assistant, Lonergan Research Group, Department of Chemistry and Biochemistry, University of Oregon, Eugene, OR, 2012-2017

Graduate Teaching Assistant, Department of Chemistry and Biochemistry, University of Oregon, Eugene, OR, 2011-2017

Research Associate, Syntrix Biosystems, Auburn, WA, Sep 2010 to July 2011

GRANTS, AWARDS, AND HONORS:

Promising Scholar Award, University of Oregon, 2011

President's Scholar, Central Washington University, 2010

Science Honors Research Program, Central Washington University, 2008-2010

Dennis W. Farrell Scholarship, Central Washington University, 2007-2010

PUBLICATIONS:

D.R. Clayton, D. Lepage, P.N. Plassmeyer, C.J. Page and M.C. Lonergan, *RSC Adv.*, 2017, **7**, 7046-7051.

ACKNOWLEDGMENTS

I thank both previous and current members of the Lonergan lab for their support and mentoring. I would like to thank my advisor, Dr. Mark Lonergan for giving me the opportunity to join his research group, along with his mentorship during my time at the University of Oregon. I would like to thank my coauthors for their contributions to the work presented herein. I would like to acknowledge members of the Page and Boettcher labs for their assistance and guidance. I thank my doctoral committee: Dr. George Nazin, Dr. Catherine Page, Dr. Shannon Boettcher and Dr. Hailin Wang for their insight, questions and time.

The work reported herein was supported by the National Science Foundation under Grant No. CHE-1102637.

To my friends and family.

TABLE OF CONTENTS

Chapter Page

Chapter Page

LIST OF FIGURES

Figure Page

LIST OF TABLES

LIST OF SCHEMES

Scheme Page

CHAPTER I

GENERAL INTRODUCTION

This dissertation contains previously published and unpublished co-authored material. Chapter II was published with David Lepage, Paul N. Plassmeyer, Catherine J. Page and Mark C. Lonergan. Contributions to Chapter III were made by Mark C. Lonergan. Contributions to Chapter IV were made by Keenan N. Woods and Mark C. Lonergan.

Portions of this chapter were previously published as Clayton, D.R.; Lepage, D.; Plassmeyer, P.N.; Page, C.J.; Lonergan, M.C. Low-Temperature Fabrication of Lithium Aluminum Oxide Phosphate Solid Electrolyte Thin Films from Aqueous Precursors. RSC Adv 2017, 7, 7046-7051. The experimental work and writing was done by me. D. Lepage, P.N. Plassmeyer, C.J. Page and M.C. Lonergan provided editorial assistance.

Dissertation Goals and Objectives

Solution-phase thin-films of electronic materials are of interest for use in a variety of devices including rechargeable batteries, field-effect transistors, high-energy capacitors, electrochromics, and sensors.[1-7] The ability to produce these materials via solution-based green synthesis have resulted in a large number of studies focused on the production and incorporation of thin films into the various devices previously mentioned. In addition to single-phase materials, solution-phase thin-film synthesis enables the control of material properties through facile fabrication of metamaterials in the form of nanolaminates that are useful for energy storage applications. While a large body of

research has focused on the use of solution-phase thin-film synthesis for several metal-oxide based systems, advancing the above has not been explored for ionically conductive materials. This dissertation aims to elucidate the fundamental chemistry governing the production of high-quality, ionically conductive thin films. This work directly addresses the following goal: open the field of studying ionic conductors using solution-phase green synthesis, including the fabrication of nanolaminates that may have material properties that are not simply the superposition of the constituent materials.

This goal is achieved by addressing the following objectives:

1. The development of solution-phase synthetic methods for the production of thin-film ionic conductors.
2. The implementation of these methods for the synthesis of nanolaminates, utilizing ionically conductive constituent layers, to understand how nanostructure influences nanolaminate behavior.

This dissertation does three things: First, it provides a general overview of the properties, applications, and the various synthetic methods for the production of crystalline and amorphous solid-state electrolytes. This overview aims to provide insight into the fundamental properties of solid-state ionic conductors, their general classifications, their synthesis, and how the work presented within this dissertation fits into the larger body of scientific research. Second, a brief summary of multi-layered structures and a description of their constituent layers for the purpose of electrical storage applications is provided. This summary provides a contextual understanding of the use of

inorganic materials in multi-layered stacks resulting in new materials with interesting properties. Additionally, this summary highlights how the properties of ionically conductive thin-films make them interesting candidates for use as constituent layers for nanolaminates described in this work. Third, it describes in detail, the use of environmentally friendly aqueous solution routes for the production of amorphous thin films and the resultant characteristics of solid lithium based electrolytes and related multi-layered structures produced via these methods.

Properties and Applications of Crystalline Inorganic Solid-State Electrolytes

Inorganic Solid Electrolytes (ISEs) are a useful class of materials for a variety of electrical storage systems. The reported advantages of these materials over their liquid electrolyte counterparts include increased safety, stability and longevity. Safety concerns largely center on the the use of flammable and volatile organic solvents and in the case of lithium-based batteries, a high level of reactivity of the lithium source. The use of solid-state architecture has been proposed as a means to address these issues, with inorganic based materials serving as the focus of this work. The basic ISE is composed of a network of metal and non-metal atoms and a mobile ion. The extent of order of these networks vary among the different systems, and conductive electrolytes are often classified by their physical structure and the means with which researchers attempt to distort these arrangements.[8] These conductive materials can best be broken into two categories, crystalline and amorphous materials. Although this dissertation will focus on amorphous materials, a brief description of the major categories of crystalline materials and their associated conductivities is appropriate for context.

The basic structure of a crystalline ionic conductor is a series of ordered polyhedra composed of ions and associated ligands that together form a basic framework (see Figure 1.1).[9] The mobile ions include monovalent (Li^+, Na^+, Ag^+, K^+, Ti^+, Rb^+, Cs^+), divalent (Mg^{2+}, Zn^{2+}, Ca^{2+}, Cd^{2+}, Pb^{2+}) and trivalent (Al^{3+}, Tm^{3+}, La^{3+}) cations in addition to several anions, most notably oxygen. The polyhedra networks are composed of a wide range of metal and non-metal ions while halogens and chalcogens often serve as ligands.[9] It is the specific organization of these polyhedra which define the individual structural categories, which is largely determined by constituent atom identity in both the polyhedra and ligand. Glass et al. defines three qualities that promote ionic conductivity in solid state conductors: high disorder in the mobile ion sublattice, weakly bound mobile ions, and an open crystal structure that permits macroscopic ion movement.[10]

The mobility of the conductive ions is critical in solid electrolytes. Typically, monovalent ions are the most conductive in solid systems. A decrease in the diffusion coefficient and an increase in activation energy is associated with increased valency, as this parameter directly influences both solid solubility and ion distribution within the lattice.[11] A second factor that influences ion conductivity is mobile ion size. This parameter does not follow a specific periodic trend with respect to conduction. Individual structures are associated with different size requirements for mobile ions. Maximizing diffusion coefficients and minimizing activation energies is often attained when mobile ions are small enough to navigate the solid network unobstructed, but large enough to avoid electrostatic wells. [12] The primary energetic barrier mobile ions must overcome are bottleneck points along the conduction pathway.[13] Furthermore, the presence and manipulation of vacancies, interstitials and lattice site occupancy also influence ionic

conductivity as these factors directly impact energetic barriers that sum as the apparent activation energy.[9]

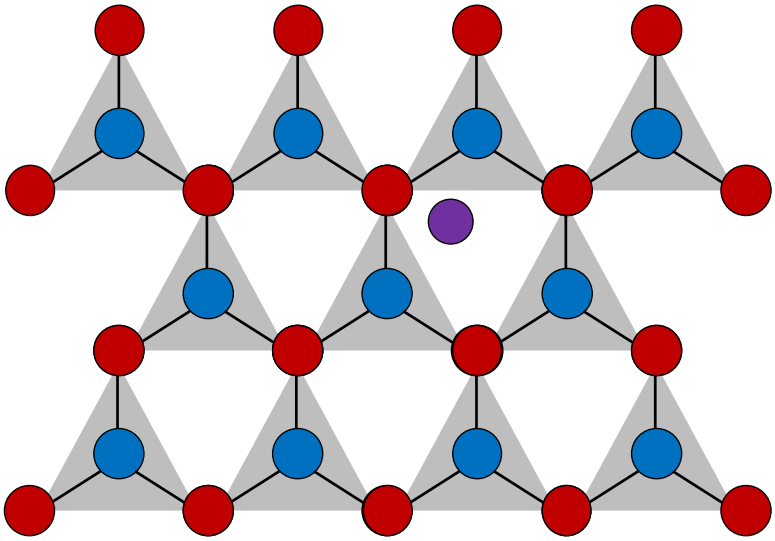

Figure 1.1. Pictorial representation of the basic structure of a crystalline ionic conductor. Mobile ions (purple sphere) move through the highly ordered polyhedra network composed of a various metal and non-metal ions (blue spheres) while halogens and chalcogens often serve as ligands (red spheres).

There have been a large number of reviews focused on ionic conductivity in solid-state ionic conductors.[1,9,14-21] The enhancement of these ionic conductivities is often system dependent. A brief discussion of the major structural classifications with specific materials and their conductivities is provided.

Although there are several classifications of crystalline solid electrolytes, the most studied systems are LISICON-like, thio-LISICON-like, NASICON-like, garnet, and perovskite. As previously mentioned, conductivities range across several orders of magnitude with no one system standing above the rest. LISICON have the general formula $Li_{2+2x}Zn_{1-x}GeO_4$ and have room temperature conductivities on the order of 1.0 x 10^{-7} S cm^{-1}. The related thio-LISICON replaces oxide ions with sulfide ions. The larger

radius of substituted S^{2-} over O^{2-} increases the radius of the lithium ion transport channels. This material is substantially more conductive with $Li_{10}GeP_2S_{12}$ having a room temperature conductivity of 1.2×10^{-2} S cm^{-1}.[22] NASICON solid electrolytes have the general formula $NaA_2^{IV}(PO_4)_3$ (A^{IV} = Ge, Ti, and Zr). These materials are highly conductive with $Li_{1.3}Al_{0.3}Ti_{1.7}(PO_4)_3$ (LATP) having a conductivity of 7×10^{-4} S cm^{-1}.[23] Garnets have the general formula $Li_5La_3M_2O_{12}$ (M = Ta, Nb). The garnet structure $Li_7La_3Zr_2O_{12}$ has a conductivity of 2.1×10^{-4} S cm^{-1}.[24] The perovskites (ABO_3) of lithium lanthanum titanate (LLTO) have some of the best conductivities of crystalline solid electrolytes. The material $Li_{3x}La_{(2/3)-x}TiO_3$ (x = 0.11) has a conductivity of 1.0×10^{-3} S cm^{-1}.[25] As previously noted a substantial amount of research is focused on maximizing conductivities within each system, and this is by no means an exhaustive list. However, it does provide a context for the materials presented in this work as these conductivities rank among the best in solid-state systems.

An important note is that ionic conductivity is often judged by order of magnitude. It is not unusual for conductivity values to range several orders of magnitude within an individual structural classification. Further, the specific structural manipulation resulting in maximum conductivity does not follow repeatable trends and is often unpredictable and unique to specific systems.[26]

Properties and Applications of Amorphous Inorganic Solid-State Electrolytes

Amorphous ionic conductors are the second major classification of solid-state electrolytes. These materials are most often defined by their high level of structural disorder. A classic example that provides insight into the mechanisms of conduction in glassy conductors are the amorphous metal oxides. Although these materials are defined

by high levels of structural disorder, a general framework is present (see Figure 1.2). In the case of amorphous metal oxides, this framework is an array of metal oxide cations associated via covalently bound bridging oxygen atoms.[27] The method of conduction in amorphous solids is often described by two models. The first model, popularized by Souquet, is the weak electrolyte model. This model works under the assumption that some of the oxygen atoms within the network do not form bridges, but instead are negatively charged and referred to as non-bridging oxygen atoms. Positively charged mobile ions are either associated with these negatively charged oxygen atoms or occupy interstitial sites and are free to conduct throughout the disordered network.[27,28] The key to controlling ionic conductivity within this model is maximizing the amount of disassociated ions without generating so much disorder that a network ceases to exist. The second model popularized by Glass and Nassau is known as the random site model.[10] In this model, a continuum of sites with varying levels of free energy are occupied by mobile ions. When a limited number of mobile ions are present, they tend to occupy sites with the lowest free energy and highest activation energy. Only after these sites are filled can higher energy sites, more conducive to conduction, be occupied. The greater the percentage of mobile ions located within these higher energy sites, the more likely high levels of conductivity are observed. As in the weak electrolyte model, a higher number of mobile ions is key to high levels of measured ionic conductivity. Without an adequate number of mobile ions able to occupy the sites described above, measurable ionic conductivity is not observed.

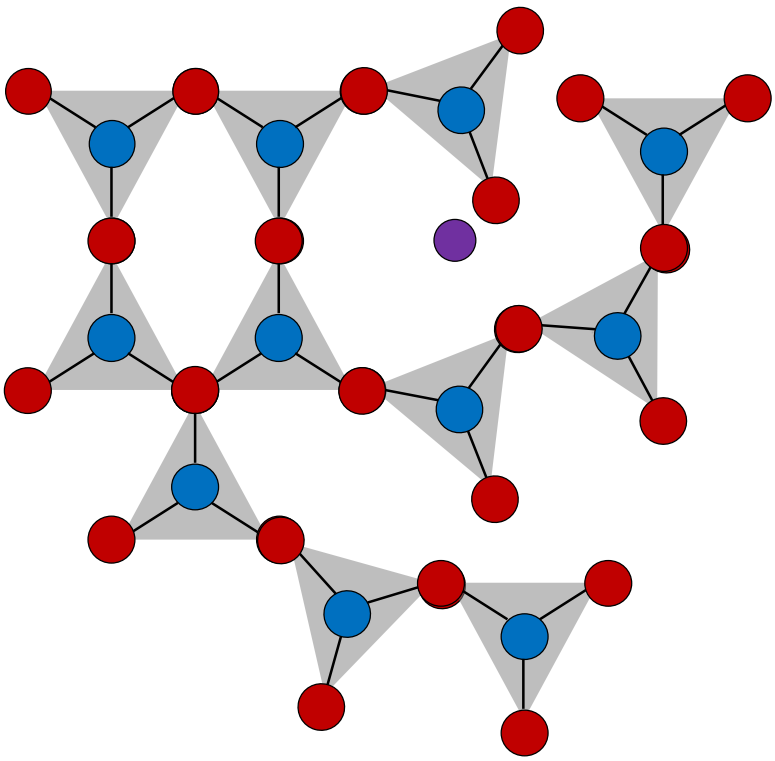

Figure 1.2. A pictorial representation of an amorphous metal oxide ionic conductor. Mobile ions (purple spheres) move thorough a highly disordered framework of metal oxide cations (blue spheres) associated via covalently bound bridging oxygen atoms (red spheres).

One of the attractive features of amorphous glasses is that they commonly possess higher conductivities compared to that of their crystalline form.[29-31] One explanation for this behavior is that amorphous materials are free of grain boundaries, which often limit the conductivity of their crystalline counterparts. A second attractive feature found in amorphous materials is that the high level of disorder, which is responsible for increased ion mobility in glasses, reduces the amount of electronic state overlap of neighboring atoms, ultimately reducing their electronic conductivity.[10] This is especially important in battery systems where high levels of electronic conductivity results in shorting between the anode and cathode, ultimately resulting in direct discharge of electrons through the electrolyte rather than an external circuit. Finally, and most importantly with respect to

this work, amorphous materials are more readily fabricated in thin film form.[8] This is particularly important for their incorporation into more complex structures including nanolaminates, which are discussed in Chapter IV of this work.

The primary categories of amorphous conductors are oxide glasses, sulphide glasses, and LIPON. The oxide glasses are a largely ignored category of solid electrolyte due to their relatively low conductivity values, which are on the order of 10^{-8} S cm^{-1}. Despite their moderate conductivity, these materials possess interesting properties and warrant further investigation for use in a variety of systems as presented herein (Chapter III). The sulphide glasses tend to have higher conductivity values over the oxide glasses with the GeS_2+Li_2S+LiI+Ga_2S_3 having a conductivity of 1 x 10^{-3} S cm^{-1}, ranking this material among the most conductive solid-state electrolytes, crystalline or amorphous, to date.[32] LIPON has a lower conductivity value of 3.3 x 10^{-6} S cm^{-1}.[33]

Inorganic Solid-State Electrolyte Synthesis

The synthesis of solid-state electrolytes varies widely depending on individual material and desired conductor form. Perhaps the most basic and widespread synthetic method is a traditional solid-state synthesis, colloquially referred to as the heat and beat method. Although this method ranks low in terms of sophistication, it is highly effective and responsible for many of the most conductive solid electrolytes known today. The general steps involve the following: mixing of powder precursors usually through mechanical milling, pressing mixed precursors into desired form often in the form of pellets or disks, and a heat treatment in a high temperature furnace, often between 500-2000 °C, for extended periods.[34] This method is often limited due to the slow nature of

the synthesis and the high levels of inhomogeneity at the atomic scale. A sub-category of this traditional synthetic method specifically used for the synthesis of amorphous materials is melt quenching. In this method, precursor materials, often in powder form, are mixed as described in the traditional heat and beat method. Their temperature is raised to produce a molten mixture of precursors. This melt is rapidly quenched resulting in the desired material. While these methods are effective for the synthesis of highly conductive materials, use in consumer electronics requires solid-state electrolytes to be produced in compact form.

Thin-Film Synthesis of Inorganic Solid-State Electrolytes

A significant amount of research has gone into the production of solid-state electrolytes in thin-film form for compact device structure and improvement of electrolyte conductance. For these types of materials, vapor deposition methods dominate. The two major categories of vapor deposition are physical vapor deposition (PVD) and chemical vapor deposition (CVD). Physical vapor deposition involves the vaporization and transport of source material in the gas phase and subsequent condensation onto solid substrates, usually under high vacuum.[35] The major categories of physical vapor deposition include vacuum deposition, which has a direct line-of sight transport of gas material from source to substrate and sputtering in which a physical source (target) is bombarded with ions, dislodging source material which can then condense on the substrate.[35] Chemical vapor deposition involves the flow of precursors in gaseous form into a reaction chamber. Here gases react and are deposited onto desired substrates. A highly advanced method of CVD is known as atomic layer deposition

(ALD). In this method source vapors are alternately deposited one at a time, resulting in monomolecular layer depositions.[36] This results in highly dense, uniform films, with unparalleled thickness control. While these methods are highly effective for the deposition of thin films, problems including slow deposition times, heat induced structural damage, limitations of substrate identity, and film inhomogeneity have been associated with these methods. Furthermore, the requirement of advanced vacuum apparatuses makes these methods very expensive. Ultimately, these issues have resulted in the development of alternative synthetic methods for thin-film deposition that are quick, low cost, and address limitations of vapor deposition.

Solution-Phase Thin-Film Deposition of Solid-State Electrolytes

One such alternative method to the synthesis of solid electrolytes that aims to solve the issues associated with traditional processing methods, including the issue of inhomogeneity, is sol-gel synthesis. In this method, a homogenous liquid solution of precursors is generated. Through the hydrolysis and condensation of metal alkoxide or citrate precursors and organic solvents, a sol, or colloidal suspension, is generated.[37] The sol is then slowly dried resulting in transparent, usually amorphous, solid gels. A final high-temperature calcination to remove volatile compounds results in the final solid product. A major drawback of sol-gel synthesis is the use of organic stabilizing agents and solvents that must be expelled from the resultant product.[38] The removal of these substance often result in cracking and void formation.[39,40]

For films to be used in devices, they must be crack free and clear of large voids. This means that in order for a solution process to be useful, the transition from

homogeneous precursor solution to film must be conducive to quality film formation. This is an obvious short-coming of sol-gel synthesis directly related to the use of stabilizing and chelating agents necessary for completely solvated precursors. The removal of these species are associated with cracking and void formation.[39,40] Furthermore, the temperatures required to drive off volatile agents also generate highly porous films with high levels of roughness, directly linked with the large volume loss during the drying process of wet gels.[41]

An alternative approach to sol-gel chemistry is the solution process prompt inorganic condensation (PIC). PIC is based on the use of aqueous precursors consisting of simple inorganic salts or clusters that concentrate during spin coating, and rapidly condense to form metal oxide networks with low-temperature annealing. Unlike sol-gel synthesis, low temperature annealing nondestructively dehydrates films and releases small inorganic counterions resulting in high quality films. In addition to the small size of these counterions, compared to that of the stabilizing agents utilized in sol-gel, their identity is specifically targeted for low-temperature, non-disruptive decomposition. The success of PIC is predicated on the complete dissolution of precursor salts and the resultant homogeneous nature of the precursor solutions. In this work, aqueous solutions containing Al^{3+} are used. The use of aluminum solutions is common to PIC chemistries and has been extensively studied.[42-46] A key attribute of aluminum solutions that ultimately yield quality films is the hydrolysis and condensation of solvated Al^{3+}, which produces molecular hydroxo clusters.[47,48] In the presence of oxyanion groups, these hydroxo clusters result in the formation of heteropolymeric species.[42,49] As with other PIC chemistries, mild heating initiating the decomposition and non-disruptive elimination

of counterions along with the simultaneous dehydration of solvent produces a stable oxide framework.[50-52]

Chapter II will describe the first reported solution deposition of the ionically conductive thin-film LiAlPO via PIC. The synthesis utilizes aluminum, phosphate, and lithium precursor solutions for the deposition of high quality films (see Figure 1.3). The fabrication of these films are enabled by the low temperature dehydration and elimination of nitrate counterions. The successful synthesis of these films provides a stage for the successful deposition of solid-state electrolytes using PIC chemistries.

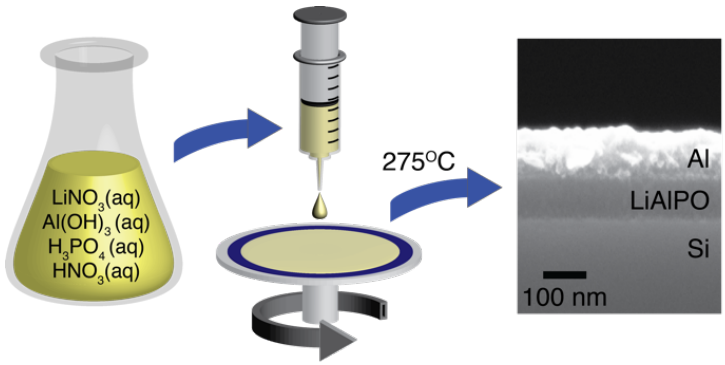

Figure 1.3. Pictorial representation of PIC chemistries including aqueous solution precursors and spin processing of a LiAlPO film.

Portions of this work were previously submitted to publish as Clayton, D.R.; Lepage, D.; Plassmeyer, P.N.; Page, C.J.; Lonergan, M.C. Low-Temperature Fabrication of Lithium Aluminum Oxide Phosphate Solid Electrolyte Thin Films from Aqueous Precursors. The writing and experimentation was done entirely by me. D. Lepage, P.N. Plassmeyer, C.J. Page and M.C. Lonergan provided editorial assistance.

Multi-Layered Structures

As previously mentioned, inorganic materials have received considerable interest for use in a variety of electrical systems. This interest is in large part due to their reputation for high levels of chemical and thermal stability.[53] The chemical composition and atomic arrangements ultimately determine the electrical properties of these materials which behave as insulators, semiconductors, and conductors.[54] A particular material parameter of interest resulting in high levels of interest over years is the large dielectric constant associated with some metal oxides. Unfortunately, these materials often exhibit high levels of leakage currents and high reactivity against metal contacts.[55] Initial attempts to improve individual material characteristics focused on the use of additives to address specific shortcomings including leakage current.[56-58] Although these additives often possessed ideal material parameters that the host material was deficient in, their incorporation ultimately reduced the positive attributes of the original structure, with respect to the material's proposed application. [59] An alternative approach is the use of multi-layered stacks to merge specific characteristics, beneficial for the intended application, into a single material form. Ultimately, these hybrid materials aim to exhibit high levels of stability and superior electrical characteristics. A significant body of research has focused on the use of nanolaminates, which are layered composites of alternating materials. Typically each layer is a thin film of under 100 nm composed of at least two different materials with the resultant structures often exhibiting characteristics unique from their single layer constituents.[53] As with single layer films, composition ultimately determines material parameters. An attractive attribute of nanolaminates is that the dimensions of the individual layers strongly impact the physical and chemical

properties. This phenomenon is most commonly observed when layer thickness falls below the length scale that governs the material property. Park et al demonstrated that the sublayer thickness directly impacts dielectric constant with a drastic increase in the value of *k* as a function of decreasing sublayer thickness.[60] This highlights the importance of synthetic methods that offer tight control over deposited film thickness. Furthermore, layer-layer interactions impact the microstructure of the nanolaminate and can be used to manipulate composition and ultimately properties.[53] This was demonstrated by Li et al in which the dielectric constant was increased through the modification of layer composition at the AlO_x-TiO_x interface.[61] In addition to composition and layer thickness, nanolaminate design scheme plays an important role in the behavior of the stack.[61-63] A simple example is the Al_2O_3-ZnO system in which the layer structure allowed for the tuning of electrical properties beyond the range of either constituent material.[64,65] As previously mentioned, metal oxides often exhibit high values of dielectric permittivity, ε_r, but also have low potential dielectric strength, E_{BD}. Several studies have successfully demonstrated nanocomposite materials as a means to improve breakdown strength while retaining high permittivity.[54,66,67] Jogi et al also demonstrated the ability of nanolaminates to improve leakage current as a function of layer thickness.[63]

The use of nanolaminates goes beyond the improvement of individual layer performance. The laminate structures themselves display interesting characteristics including large dielectric constants beyond 1000.[68] This represents an increase of over 700 times in the dielectric constant for the Al_2O_3-TiO_2 laminate over that of Al_2O_3.[68] Taken together, the use of nanolaminates to generate large dielectric values and high

dielectric strength can be valuable when considering the energy density capacity of a material according to equation: $W = \frac{1}{2}\varepsilon_0\varepsilon_r E_{BD}^2$

Chapter IV focuses on the synthesis of nanolaminates precisely designed to maximize the energy density as previously demonstrated in several studies.[66,69,70] Specifically, this chapter focuses on the use of PIC chemistries as a sustainable approach to the design and fabrication of quality nanolaminates with interesting material properties. The successful synthesis of quality nanolaminates via PIC has been demonstrated with the unique ability generate new materials with unique compositions or compositionally graded films.[47,71] This work aims to extend the synthesis of nanolaminates via PIC to include ionically conductive constituent layers which are known to generate large capacitance values as demonstrated in Chapter III.

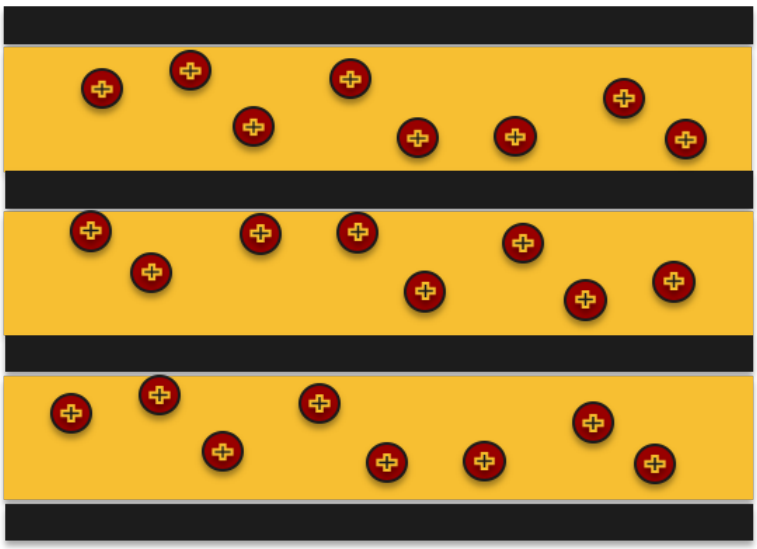

Figure 1.4. Pictorial representation of a nanolaminate stack with ionically conductive constituent layers (yellow) interspersed with non-conductive layers (black).

Portions of this work include co-authored material. Coauthored material of Chapters III and IV were completed with M.C. Lonergan. The excerpts to be included were written entirely by me. The experimental work was also performed entirely by me. M. C. Lonergan provided experimental direction and editorial assistance.

Bridge

This chapter provided a background for the applications, classifications, properties, and synthesis of inorganic solid-state electrolytes. Specifically, this chapter addressed solution phase thin film synthesis as a means to produce high quality, ionically conductive materials useful for energy storage applications. This general information provides context for this work and highlights the specific goals and general contributions of this dissertation to the scientific community. Chapter II will demonstrate the use of these aqueous solution based chemistries for the fabrication of inorganic thin-film solid-state electrolytes. It will be demonstrated that high quality thin films of the ionic conductor lithium aluminum oxide phosphate can be produced via low energy methods described in Chapter I.

CHAPTER II

LOW-TEMPERATURE FABRICATION OF LITHIUM ALUMINUM OXIDE PHOSPHATE SOLID ELECROLYTE THIN FILMS FROM AQUEOUS PRECURSORS

This chapter contains previously published and co-authored material. The experimental work and writing was done by me. D. Lepage, P. Plassmeyer, C. Page and M. Lonergan provided editorial assistance.

Introduction

Thin films of inorganic solid electrolytes (ISEs) have received considerable interest in recent years for use in a variety of devices including rechargeable batteries, electrochromics, electrolyte-gated transistors, high-energy capacitors, sensors, and other electrochemical devices.[1-7,9,17] The reported advantages of ISEs include increased safety, reliability, and thermal stability.[9,16,17,72] Thin films are needed for compact device structures and to improve electrolyte conductance. Methods for the fabrication of thin film ISEs, however, are primarily limited to expensive vacuum deposition techniques and/or require high temperature annealing, which is energy intensive and hinders integration with materials of low thermal stability.

We demonstrate herein the use of prompt inorganic condensation (PIC) as a low-temperature, solution-cast route to high quality thin films of the solid electrolyte $Li_5Al_2O(PO_4)_3$ (LiAlPO) using only aqueous precursors. PIC is a powerful approach that has been developed for the synthesis of oxide thin films.[47] It is based on the use of

aqueous precursors consisting of simple inorganic salts or clusters that concentrate during spin coating, and rapidly condense to form metal oxide networks with low-temperature annealing, with further dehydration and possibly decomposition of small inorganic counterions at moderately elevated temperatures. To date, PIC has been primarily used in the synthesis of thin-film oxide dielectrics, semiconductors, and nanolaminates of these compounds.[42,46,50,52,73,74] This is the first demonstration of its use for the synthesis of thin film ISEs.

Bulk LiAlPO has been previously synthesized by classic melt quenching techniques requiring temperatures in excess of 750 °C.[75] To date, thin films of this material have not been reported. By using PIC, we are able to greatly reduce the processing temperatures, and prepare this material readily in thin-film form. Previously, PIC has been used to prepare aluminum oxide phosphate thin films with P:Al ratios ranging from 0.5 to 1.0.[42] The extension of this work into the synthesis of lithium alumino phosphate glasses with a higher P:Al ratio (1.5:1) and added lithium demonstrates the flexibility of the PIC method to produce amorphous films over a range of stoichiometries.

Although LiAlPO has not been previously synthesized by a solution-based approach, other ISEs have. However, most currently available approaches that produce quality ISE thin films employ environmentally harsh solvents, such as hydrazine, or rely on organic ligands and/or solvents.[76,77] For example, sol-gel synthesis typically utilizes metal alkoxide or citrate precursors and organic solvents. The removal of these solvents and ligands result in undesirable film characteristics including cracking and void formation.[40,78] Although PIC requires the liberation of water and possibly counterion

decomposition products, cracking and surface roughness are not commonly observed in films prepared by this method.[42,74] Further, in many cases the removal of water and counterions can be achieved at low temperatures, as in the present study.[42,74] Moreover, the use of water as a solvent has obvious benefits in terms of sustainability and hazard reduction. Previous reports of thin-film ISEs from aqueous solutions are exceptionally limited. Most closely related to the work herein is that of van den Ham et al, who reported an aqueous precursor route to thin films of an amorphous lithium lanthanum titanate perovskite ISE.[79] These authors used an aqueous citrate-peroxo-Ti(IV) precursor, which required annealing temperatures of 500 °C for complete decomposition and elimination of citrate. Here we demonstrate that PIC using nitrate and phosphate precursors can be used to synthesize dehydrated, smooth, uniform LiAlPO films at temperatures as low as 275 °C.

Experimental

Precursor Synthesis

The LiAlPO precursor solution was prepared with the addition of 50 mmol $Al(OH)_3 \bullet xH_2O$ (Alfa Aesar) to 50 mL of 18 MΩ H_2O. The level of hydration in $Al(OH)_3 \bullet xH_2O$ was determined gravimetrically through thermal conversion to the oxide (Al_2O_3). Complete dissolution was achieved following the addition of 100 mmol of HNO_3 (EMD Chemicals 70% w/w) with one hour of stirring at 80 °C. To the clear solution 75 mmol of H_3PO_4 (EMD Chemicals 85% w/w) was slowly added. The solution was stirred overnight with heating (80°C). The solution was allowed to cool to room temperature and 137.5 mmol of solid $LiNO_3$ (Alfa Aesar) was added. The mixture was

stirred at room temperature until complete dissolution of the $LiNO_3$ (~10 minutes). The solution was diluted with 18 MΩ H_2O to achieve a 0.4 M concentration with respect to Al. The P:Al:Li ratio was 1.5:1:2.5 for all precursor solutions. This concentration of precursor solution was used for all characterization with the exception of FTIR analysis for which films were prepared with solutions of 0.7 M with respect to Al.

Film Deposition and Device Fabrication

All of the films were prepared by solution deposition of a single layer via spin-processing. Boron doped Si substrates (0.008-0.020 Ω cm) were sonicated in a five percent Contrad 70 solution for 60 min at 50 °C. Substrates were then treated by plasma cleaning to produce a hydrophilic surface (120 s O_2/N_2 plasma etch using a Plasma Etch, Inc. PE-50 Benchtop Plasma Cleaner set to maximum power). The precursor solution was filtered (2x) through a 0.45 μm Teflon filter. Substrates were flooded with the filtered LiAlPO precursor solution via syringe and spun at 3000 rpm for 30 s. An immediate hot plate cure at 275 °C took place for one minute. A final anneal at either 275 or 400 °C was then carried out for one hour. An array of circular (0.011 cm^2) Al top contacts were thermally evaporated onto the LiAlPO surface via shadow mask. An Al plate adhered by silver print to the silicon wafer was used for a back contact.

Characterization

Weight loss and thermal stability of evaporated LiAlPO precursor powders were analysed using a TA Instruments Thermogravimetric Analyzer (TGA Q500). Further thermal characterization was conducted using a TA Instruments Differential Scanning

Calorimeter (DSC-2920). For these measurements, the precursor solution was evaporated at 100 °C for one hour yielding 10-30 mg powder samples. A heating rate of 2-10 °C/min from room temperature to 600 °C was completed for TGA analysis. DSC measurements were completed using a heating rate of 10 °C/min from room temperature to 460 °C.

X-ray reflectivity and diffraction measurements on film samples were collected on a Bruker AXS D8 Discover diffractometer with Cu Kα radiation to determine the total film thickness and confirm amorphous character. The chemical characteristics of the LiAlPO films were investigated by transmission Fourier transform infrared spectroscopy (Thermo Scientific Nicolet 6700 FT-IR Spectrometer) and X-ray photoelectron spectroscopy (Thermo Scientific ESCALAB 250 X-ray Photoelectron Spectrometer). All binding energies were referenced to the C 1s peak of carbon at 284.8 eV. NIST and LaSurface XPS databases were used for binding energy assignments. Film morphology and thickness were characterized using a ZEISS Ultra-55 Scanning Electron Microscope. Impedance spectroscopy measurements were performed using a Solartron 1260 Impedance Analyzer and 1296 Dielectric Interface over the frequency range 10 mHz to 1 MHz. Temperature control was achieved using a Sun Electronic Systems Environmental Chamber (Model EC1X). The apparent relative permittivity $\varepsilon_{app} = \varepsilon'_{app} - i\varepsilon''_{app}$ and conductivity $\sigma_{app} = \sigma'_{app} + i\sigma''_{app}$ were calculated from the raw complex impedance Z in the standard manner: $\varepsilon_{app} = \sigma_{app}/i\omega\varepsilon_0 = L/i\omega AZ\varepsilon_0$ where ε_0 is the vacuum permittivity. The dielectric loss tangent $\tan\delta = \varepsilon''_{app} / \varepsilon'_{app} = \tan(\theta + \pi/2)$, where θ is the measured phase angle, was also calculated.

Results and Discussion

The PIC synthesis of LiAlPO thin films reported herein involves spin casting an aqueous solution of salts and acids with appropriate stoichiometry followed by mild heating to produce an amorphous oxide film according to the following idealized chemical reaction:

$$2Al(OH)_3(aq) + 4HNO_3(aq) + 5LiNO_3(aq) + 3H_3PO_4(aq) \rightarrow$$
$$Li_5Al_2O(PO_4)_3\ (s) + 9HNO_3 + 5H_2O.$$

Scheme 2.1. Idealized chemical reaction for the synthesis of LiAlPO.

Note that nitric acid is added to solubilize the $Al(OH)_3$. Ideally, the nitric acid product is liberated as its azeotrope with water at relatively low temperature (boiling point 121 °C), but some nitrate incorporation into the LiAlPO product is also likely to occur. To explore this further, thermal analysis was first performed on bulk powders of dried precursor solution. Specifically, a solution containing $Al(OH)_3$ (solubilized with HNO_3), H_3PO_4, and $LiNO_3$ in the molar ratios of Scheme 2.1 was evaporated to near complete dryness at 100 °C. Figure 2.1 shows TGA-DSC analysis of the resulting powder. Beginning near 100 °C, there is an initial mass loss of nearly 20% accompanied by a broad endotherm. This is assigned to the continued dehydration of the powder and the elimination of nitrate from the film as the H_2O/HNO_3 azeotrope. Above 120°C in the tail of the endotherm, mass loss continues at a relatively constant and more gradual rate, with the exception of two small features in the TGA. One corresponds with a sharp endotherm at 255 °C, which coincides with the melting temperature of $LiNO_3$. The

second has an onset of 340 °C, and we assign it to the decomposition of residual nitrates in the film. This assignment is supported by IR data on thin films discussed below and indicates that nitrates are not completely removed via the H_2O/HNO_3 azeotrope evaporation, at least in bulk powders. For comparison, the decomposition of simple nitrate salts of the main group elements can occur over a wide range of temperatures from as low as 170 °C for pure aluminum nitrate to 640 °C for pure lithium nitrate. [80]

The thermal analysis data on bulk powders motivated us to study LiAlPO thin film formation at temperatures of 275 °C and 400 °C. Although dehydration, condensation, and nitrate decomposition are likely different in spin-coated thin films relative to bulk powders, we expected that these temperatures would be sufficiently high to result in near complete dehydration as well as to enable comparison of the effects of residual nitrate in the film.

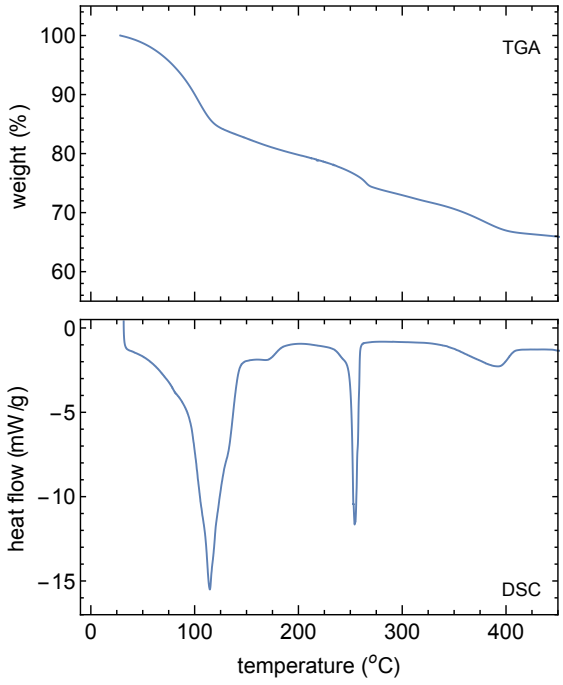

Figure 2.1. TGA and DSC curves of a LiAlPO precursor powder from 20 to 450 °C.

Thin films were made by first spin casting a precursor solution of the same composition used in the thermal analysis experiments onto cleaned silicon substrates, followed by rapid annealing at either 275 °C or 400 °C on a hot plate.

Films annealed at both temperatures were determined to be amorphous by XRD. This is consistent with the crystallization temperature for LiAlPO of greater than 500^{o}C reported by Reddy et al.[81] Amorphous films are desirable to maintain transparency and to prevent localized current pathways associated with grain boundaries in crystalline materials. The formation of amorphous films illustrates how PIC is distinctly different from the simple co-precipitation of aqueous salts. Slow heating to 275 °C of the dried LiAlPO precursor solution produced powders with diffraction peaks indicative of tridymite and cristobalite $AlPO_4$.[42] The resistance to crystallization in the PIC method is attributed to prompt dehydration and condensation to form an initial glass network during spin coating and rapid annealing.

To better understand the formation of LiAlPO thin films using PIC, FTIR spectra were collected as a function of annealing temperature (see Figure 2.2). Several peaks were monitored to confirm formation of the alumino-phosphate network and track changes in composition. Remarkably, absorption near 3600 cm^{-1} and 1640 cm^{-1} attributed to the presence of water were not observed, even after annealing at 275 °C for only one minute. This is in contrast to thin films of a different P:Al ratio, $Al_2O_{3-3x}(PO_4)_{2x}$ (AlPO) produced via PIC in which films of similar thickness show detectable water absorptions up to 600 °C.[42] Peaks in the 1200-1700 cm^{-1} are assigned to nitrate deformation vibrations. They were observed in the 275 °C annealed sample but not in the 400 °C sample indicating near complete nitrate decomposition had occurred in the latter. This

supports the assignment above of the DSC endotherm to nitrate decomposition at 340 °C. The strong peak located at 1120 cm^{-1} is attributed to the phosphate absorption band and is present at both annealing temperatures. Peaks between 400-950 cm^{-1} are associated with both Al-O and P-O vibrations.[42,82]

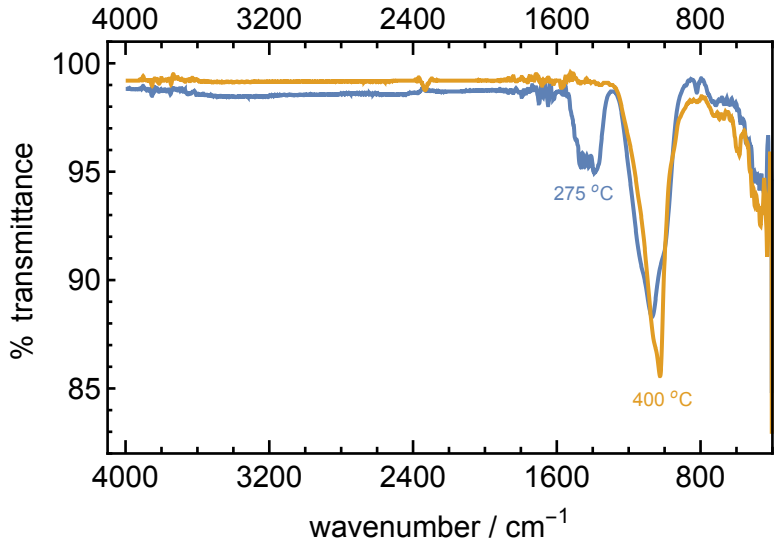

Figure 2.2. FTIR spectra of 120 nm LiAlPO films annealed at 275 °C (blue) and 400 °C (orange) for one hour.

Thin-film chemical composition was further analysed via XPS. A survey scan revealed the presence of Li, Al, P, C, N, and O (Figure AA1). The observed ratios of Li:Al:P:O match that of the precursor solution in samples processed at 275 °C and are presented in Table S1. It is noted that adventitious carbon was observed in all of the films due to air exposure with the C 1s peak at 284.8 eV serving as a charge correction reference.

The relative oxygen content did not change over a range of annealing conditions consistent with near complete dehydration of the film by 275 °C. As shown Figure 2.3, the O 1s peak shape was somewhat different between the 275 °C and 400 °C samples.

The shape at 275 °C was best fit with a convolution of peaks corresponding to $AlPO_4$ (531.7 eV), H_2O (533.3 eV) and OH^- (530.9 eV), whereas at 400 °C, the O 1s signal is entirely attributed to $AlPO_4$. The relatively minor contribution of H_2O and OH^- to the O 1s XPS signal, the constancy of the relative oxygen content by XPS between the 275 °C and 400 °C samples, and the absence of water vibrations in the IR suggest that the film is nearly completely dehydrated at 275 °C.

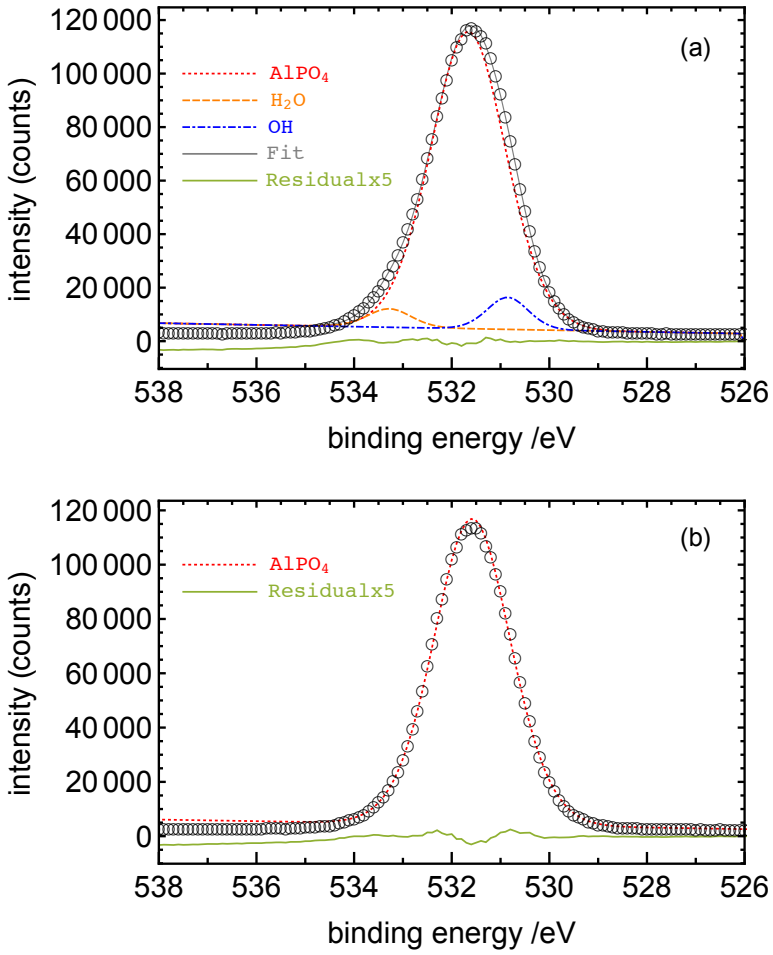

Figure 2.3. XPS spectra of the O 1s peak of LiAlPO films as a function of annealing temperature: (a) 275°C and (b) 400 °C. Experimental data (open circles), $AlPO_4$ fit (red), H_2O fit (orange), OH fit (blue), and residual fit (green).

XPS data indicates the ratio of nitrogen to aluminium in films annealed at 275 °C is 1:10 suggesting most residual nitrogen has been eliminated by this temperature. Furthermore, the N 1s signal was extremely weak suggesting minimal nitrogen content. Annealing at 400 °C resulted in the continued reduction of the N 1s peak supporting elimination of nitrate stretches as observed by FTIR. The single Li 1s peak located at 55 eV is indicative of lithium in a phosphate environment and inconsistent with that of lithium oxide (53 eV).

Scanning electron microscope (SEM) images shown in Figure 2.4 demonstrate the high quality of the deposited films with respect to smoothness, density, and porosity. No apparent cracking or obvious film disruptions are observed despite the high volume of water loss required for film formation. We propose that the initial conversion of metal hydroxides in the precursor solution to metal oxide networks during film formation is a relatively forgiving transition that alleviates stress. Additionally, the ease with which decomposed counterions are expelled from the film prevents the high level of porosity observed in organic precursor systems. This is in stark contrast to that typically observed in more traditional sol-gel methods based on organic precursor systems. The fact that only relatively small molecules, such as H_2O, HNO_3 or NO_2 from nitrate decomposition, need be expelled is believed to contribute to the formation of compact films with little porosity.

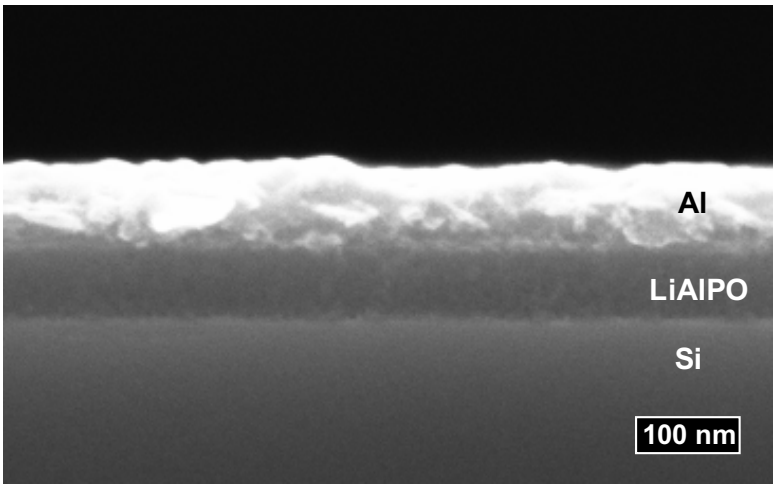

Figure 2.4. Cross-sectional SEM image of LiAlPO film annealed at 275 °C for one hour.

The thickness of films produced can be readily controlled by adjusting precursor solution concentration and spin speed. In this work, single layer films from 20 nm to 150 nm were fabricated from 0.1 M to 0.8 M precursor solutions, respectively (Figure AA2). These results are consistent with other studies of Al-P-O films produced using PIC. [43] Lithium ion conductivities of the LiAlPO films were determined using impedance spectroscopy. Figure 2.5 shows the resulting dielectric functions measured at room temperature. The real part of the apparent conductivity, σ'_{app}, as a function of frequency yields a small plateau region where the DC ionic conductivity was determined. As the Al and Si electrodes are blocking to lithium ions, polarization of ions at the electrode-electrolyte interface is indicated by capacitive behaviour at low frequency. The plateau region observed at intermediate frequencies is attributed to the bulk resistance of the solid electrolyte film. The separation of capacitive ion polarization at low frequency from a potentially frequency dependent conductivity makes rigorous extraction of the DC conductivity challenging and model dependent.[83] For consistency, we take the conductivity at the frequency corresponding to the peak in the dielectric loss as an

estimate of the DC ionic conductivity, as has been done in other systems.[84] The room temperature DC conductivity of films annealed at 275 °C was calculated to be σ_{DC} = 2.6 x 10^{-8} S cm^{-1} for 74 nm films. This conductivity is comparable to the literature value of 2.8 x 10^{-8} S cm^{-1} for bulk glasses of nominally the same composition, but prepared using high temperature methods.[81] While we recognize that the conductivity is below that of other solid electrolytes currently used in battery research, it should be noted that the level of conductivity was maintained with the use of a more environmentally sustainable approach. Furthermore, the method of synthesis provides ample opportunity to improve conductivity through chemical modification as discussed below. Activation energies were determined by plotting log σ_{DC} versus $1/T$ according to the Arrhenius equation: $\sigma = A \exp[-E_a/(kT)]$ where A is the pre-exponential factor, E_a is the activation energy, k is the Boltzmann constant, and T is temperature. The value of E_a extracted from the linear fit of the log σ_{DC} versus $1/T$ is 0.67 eV, consistent with that reported for bulk LiAlPO.[81]

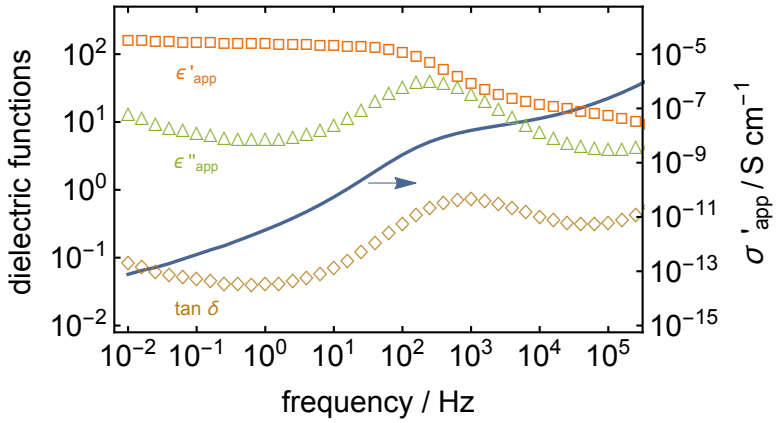

Figure 2.5. Impedance data at 23 °C of a 74 nm thick LiAlPO films annealed at 275 °C. The real part ε'_{app} (orange squares) and imaginary part ε''_{app} (green triangles) of the apparent relative permittivity, the real part of apparent conductivity σ'_{app} (blue line, right ordinate), and the loss tangent tan δ (brown diamonds).

The real part of the apparent permittivity (ε'_{app}) as a function of frequency and temperature is shown in Figure 2.6. The low frequency side is assigned to the polarization of ions against the blocking electrodes, and yields a large value $\varepsilon'_{app} = 100$ for a 68 nm film. Consistent with this assignment is the fact that the low frequency ε'_{app} is observed to depend on the thickness of the film. This is because the characteristic length of the ionic double layer is the Debye length of the electrolyte, rather than the thickness of the film. The ionic polarization necessary to form an electrode double layer results in a constant contribution to the capacitance, regardless of film thickness, which manifests as a thickness dependent ε'_{app}. The high frequency dielectric constant is near 6, which is slightly above that of AlPO, and it is thickness independent.[43] In addition to the long-range motion of lithium ions that contribute to ionic double layer formation at the electrodes, lithium displacements over shorter ranges contribute to the bulk dielectric constant at higher frequencies leading to an increased dielectric constant relative to AlPO.

The large double layer capacitance of thin-film ISEs has led to interest as gate dielectrics in field-effect transistors.[7,85] Primarily, these studies have focused on monovalent cation incorporation into aluminium oxide materials resulting in sizeable capacitance and a subsequent reduction in operating voltages.[7,85-87] Specifically, Liu et al observed an increased capacitance in alkali metal ion incorporated alumina used as gate dielectrics for oxide field-effect transistors. The standard alumina films had a low frequency capacitance of 0.13 $\mu F\ cm^{-2}$. Incorporation of lithium into the alumina increased that value to 1.8 $\mu F\ cm^{-2}$. Our lithium incorporated alumina phosphate has a

low frequency capacitance of 1.6 μF cm^{-2}, suggesting these films might be of interest for this application.

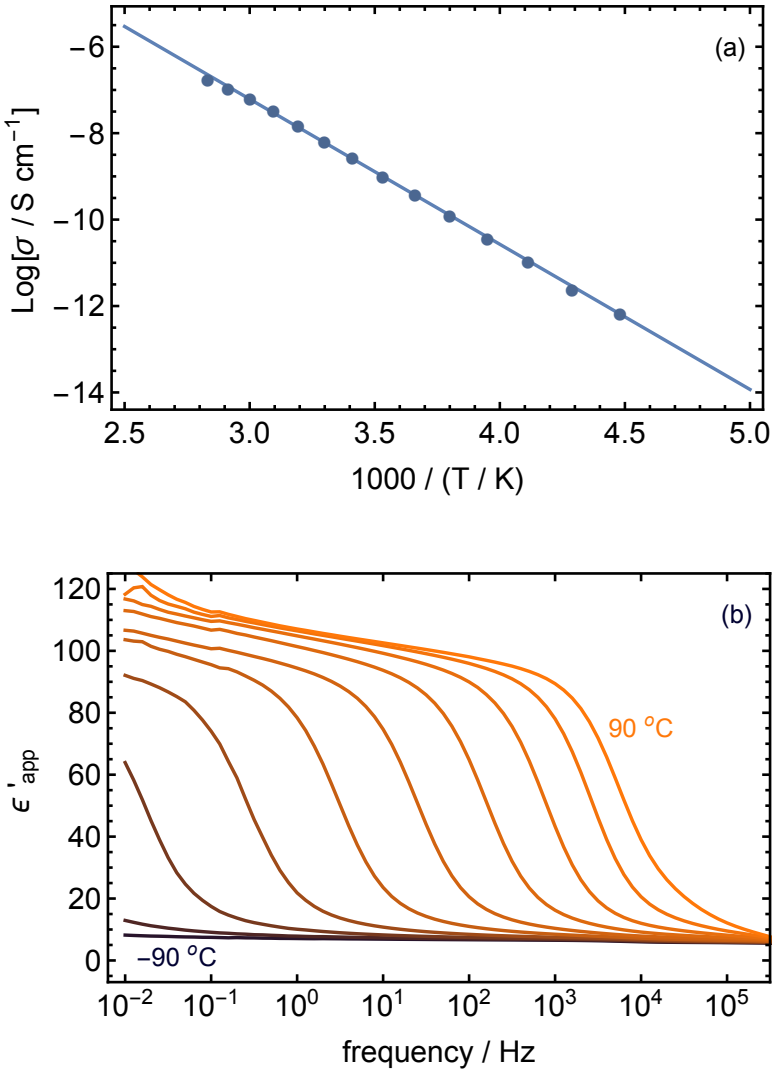

Figure 2.6. (a) Arrhenius plot of the DC conductivity σ_{DC} value at the peak in the loss tangent tan δ frequency from 74 nm thick LiAlPO film and (b) Frequency dependent ε'_{app} as a function of temperature over the range -90 °C to 90 °C in 20 °C increments for the same sample.

The ionic conductivity of the LiAlPO films is directly linked to annealing conditions. We postulate that the rapid dehydration associated with PIC prevents rigid

organization within films resulting in non-bridging oxygen atoms with which Li ions are able to associate to give a non-random hopping mechanism of conduction.[88,89] However, the actual annealing temperature is also important. Annealing at 400 °C resulted in a reduction in observed ionic conductivity ($\sigma = 1.6 \times 10^{-10}$ S cm^{-1}). This result is expected when considering the spectroscopic data and the proposed mechanism of ion conduction. The O 1s XPS peak at elevated annealing conditions is entirely assigned to $AlPO_4$ suggesting the elimination of non-bridging oxygen atoms necessary for lithium ion conduction. At these annealing conditions, the inorganic condensation is pushed near completion resulting in the formation of a stable $AlPO_4$ framework. Mobile lithium ions lose association sites required for long-range motion and the resultant conductivity is significantly reduced.

Conclusions

We have reported a low energy approach to the synthesis of thin-film ISEs via aqueous solution deposition. LiAlPO thin films produced via prompt inorganic condensation demonstrate a room temperature conductivity of 2.6×10^{-8} S cm^{-1} (thickness = 74 nm) and activation energy of 0.67 eV. These values are consistent with lithium ion conduction observed in bulk LiAlPO samples but produced via energy intensive melt quenching techniques. Precise control over desired film thickness via precursor concentration was achieved with pinhole free films obtained over the 20 nm to 150 nm thickness range.

The combination of solution deposition and low temperature processing is a unique approach to the synthesis of ISE thin films. Previously, synthesis routes to lithium

alumino phosphates have been limited to melt quenching syntheses of bulk powders processed between 750 °C and 950 °C.[75,81,90] Solution based syntheses of other ISEs have required temperatures ranging from 650 °C to excess of 1000 °C.[91,92] We have successfully reduced processing conditions to 275 °C using an aqueous solution route that allows production of high quality thin-film ISEs. Reducing processing temperatures is a first step in extending the direct synthesis of ISE thin films to substrates beyond silicon and glass, such as those desired for flexible electronics. Because homogenous solution precursors are used, incorporation of additives or metal substitutions to increase film conductivity is readily achieved.[81,93] This study serves as a first step towards future work that seeks to vary composition for new solution processed ISEs as a way to maximize their conductivity. Finally, PIC allows for the direct deposition of ISEs as smooth, dense thin films that are ideal for layered systems requiring high quality interfaces such as nanolaminates, batteries, and thin film transistors, without the use of vacuum deposition. [74,85]

Bridge

This chapter demonstrated the use of PIC chemistries to produce thin-films of the ionic conductor LiAlPO. The use of PIC allows for the production of quality thin-films at significantly lower temperatures compared to that of bulk LiAlPO prepared via melt quenching. Most importantly, LiAlPO reported in this chapter retain conductivities and activation energies consistent with their bulk material counterparts. In Chapter III the use of aqueous solution processing is extended beyond the LiAlPO system described in Chapter II, to include the solid state ionic conductor Li_2O-Al_2O_3 (LiAlO). It will be demonstrated that quality LiAlO thin-films with high values of ε'_{app} can be produced.

CHAPTER III

FABRICATION OF LITHIUM ALUMINUM OXIDE SOLID ELECTROLYTE THIN FILMS FROM AQUEOUS PRECURSORS

This chapter contains previously unpublished and co-authored material. The experimental work and writing was done by me. M. Lonergan provided editorial assistance.

Introduction

Inorganic solid electrolytes (ISEs) have been identified as a promising group of materials for use in a variety of electrochemical devices. [1-7,9,17] Reported advantages include increased safety, reliability, and reduced waste.[94] A major hurdle to the incorporation of these solid-state electrolytes into electrochemical systems is their low conductivities compared to that of their liquid counterparts. One solution to improve electrolyte conductance is the use of thin films, more specifically, the use of amorphous thin films. A significant obstacle in the use of crystalline materials is the restriction of conducting ions to various paths dependent on specific crystallographic arrangements.[30] The use of amorphous materials addresses this obstacle in part, because of the large amount of structural disorder associated with glassy conductors. Furthermore, lithium ions are known to be fairly mobile species with decreasing activation energies as a function of increased structural disorder.[28] Although several studies have aimed to solve the issue of low electrolyte conductance in ISEs, fabrication methods have received less

interest. The use of expensive vacuum deposition and/or high temperature processing has dominated synthetic methods.

The synthesis of bulk LiAlO powders has traditionally been prepared by solid state methods requiring processing temperatures in excess of 1000 °C.[95,96] More recently, synthetic methods including combustion synthesis and sol-gel synthesis have produced LiAlO in powder form.[97,98] Thin films of this material have been synthesized via r.f.-magnetron sputtering and more recently atomic layer deposition (ALD).[99-101] These synthetic methods are limited by their processing conditions, equipment, and material state. As previously mentioned a high level of importance has been placed on the ability to produce electrolytes in thin film form. Synthetic methods that yield only bulk powders are insufficient in their application, particularly for use in consumer electronics. High temperature processing limits these solid-state electrolytes in terms of their material compatibility in more complex structures, especially those systems incorporating temperature insensitive elements.[102] The use of vacuum chambers restricts the deposition of these materials to substrates that fit within these chambers, eliminating these electrolytes from large-area electronics. Furthermore, synthetic methods such as ALD are notorious for slow deposition rates. A synthetic method utilizing minimal equipment, low temperature processing, and that can produce high quality thin films is of great interest.

We demonstrate herein the use of prompt inorganic condensation (PIC) as a low cost, environmentally sustainable approach to the synthesis of amorphous thin films of the ISE Li_2O-Al_2O_3 (LiAlO). PIC is a solution based deposition technique that utilizes environmentally benign solutions for the synthesis of oxide thin films.[47] In addition to the use of environmentally friendly solutions, PIC does not require the use of vacuum

deposition and high temperature processing. Most importantly, PIC has been used to deposit quality thin films for a variety of oxide materials including the amorphous solid electrolyte $Li_5Al_2O(PO_4)_3$ (LiAlPO).[103] The present study aims to extend PIC synthesis to LiAlO and investigate the chemical and electrical properties of thin films deposited via aqueous solution precursors.

Experimental

Precursor Synthesis

The LiAlO precursor solution was prepared with the addition of 10 mmol $Al(NO_3)_3 \bullet 9H_2O$ (Alfa Aesar) to 5 mL of 18 MΩ H_2O. Complete dissolution was achieved following one hour of stirring at room temperature. Separately, a solution of 10 mmol $LiNO_3$ (Alfa Aesar) in 5 mL of 18 MΩ H_2O was prepared. Complete dissolution of the $LiNO_3$ was completed after approximately 10 minutes. The clear solutions were combined and allowed to stir overnight at room temperature. The combined solution was diluted with 18 MΩ H_2O to achieve a 0.5 M concentration with respect to Al. The Al:Li ratio was 1:1 for all precursor solutions. This concentration of precursor solution was used to prepare films for characterization with the exception of FTIR analysis, which requires thicker films to detect various chemical stretches, for which films were prepared with solutions of 0.7 M with respect to Al.

Film Deposition and Device Fabrication

All of the films were prepared by solution deposition of a single layer via spin-processing. Boron doped Si substrates were sonicated in a five percent Contrad 70

solution for 5 min at 30 °C. Substrates were then treated by plasma cleaning to produce a hydrophilic surface (120 s O_2/N_2 plasma etch using a Plasma Etch, Inc. PE-50 Benchtop Plasma Cleaner set to maximum power). Single side polished (0.005-0.025 Ω cm) wafers were used for all electrical measurements while double side polished (> 3000 Ω cm) were used for FTIR measurements. The precursor solution was filtered (2x) through a 0.45 μm Teflon filter. Substrates were flooded with the filtered LiAlO precursor solution via syringe and spun at 3000 rpm for 30 s. An immediate hot plate cure at 275 °C took place for fifteen minutes. A final anneal at 400 °C was then carried out for one hour under the flow of forming gas. An array of circular (0.011 cm^2) Au top contacts were thermally evaporated onto the LiAlO surface via shadow mask. An Al plate adhered by silver print to the silicon wafer was used for a back contact.

Characterization

Weight loss and thermal stability of evaporated LiAlO precursor powders were analysed using a TA Instruments Thermogravimetric Analyzer (TGA Q500). Further thermal characterization was conducted using a TA Instruments Differential Scanning Calorimeter (DSC-2920). For these measurements, the precursor solution was dried in the TGA as an isotherm for several hours yielding 3-10 mg powder samples. This drying step was to protect instrumentation and did not negatively impact experimental results. A heating rate of 2 °C/min from room temperature to 400 °C was completed for TGA analysis. DSC measurements were completed using a heating rate of 10 °C/min from room temperature to 400 °C. A hole was poked in the DSC pan prior to measurement to prevent rupture of pan due to outgassing of the sample. X-ray reflectivity and diffraction

measurements on film samples were collected on a Bruker AXS D8 Discover diffractometer with Cu Kα radiation to determine the total film thickness and confirm amorphous character. The chemical characteristics of the LiAlO films were investigated by transmission Fourier transform infrared spectroscopy (Thermo Scientific Nicolet 6700 FT-IR Spectrometer) and X-ray photoelectron spectroscopy (Thermo Scientific ESCALAB 250 X-ray Photoelectron Spectrometer). All binding energies were referenced to the C 1s peak of carbon at 284.8 eV. NIST and LaSurface XPS databases were used for binding energy assignments. Film morphology and thickness were characterized using a ZEISS Ultra-55 Scanning Electron Microscope. Impedance spectroscopy measurements were performed using a Solartron 1260 Impedance Analyzer and 1296 Dielectric Interface over the frequency range 10 mHz to 1 MHz. Temperature control was achieved using a Sun Electronic Systems Environmental Chamber (Model EC1X). The apparent relative permittivity $\varepsilon_{app} = \varepsilon'_{app} - i\varepsilon''_{app}$ and conductivity $\sigma_{app} = \sigma'_{app} + i\sigma''_{app}$ were calculated from the raw complex impedance, Z, in the standard manner: $\varepsilon_{app} = \sigma_{app}/i\omega\varepsilon_0 = L/i\omega AZ\varepsilon_0$ where ω is the angular frequency, L is the thickness, and ε_0 is the vacuum permittivity. The dielectric loss tangent $\tan\delta = \varepsilon''_{app} / \varepsilon'_{app} = \tan(\theta + \pi/2)$, where θ is the measured phase angle, was also calculated.

Results and Discussion

PIC synthesis was utilized to synthesize amorphous oxide thin films of LiAlO. An aqueous precursor solution composed of inorganic salts was spun onto substrates followed by low temperature annealing to produce solid-state thin films. The pre-annealed metastable product is represented by the following idealized chemical reaction:

$$2Al(NO_3)_3 \bullet 9H_2O(aq) + 2LiNO_3(aq) \rightarrow Li_2O\text{-}Al_2O_3(s) + 8HNO_3 + 14H_2O.$$

Scheme 3.1. Idealized chemical reaction for the synthesis of LiAlO.

Nitric acid is expected to thermally decompose at relatively low temperatures producing gaseous NO_2.[104] The release of small molecules of NO_2 is expected to occur prior to film formation. To determine appropriate annealing conditions, thermal analysis of bulk powders from dried precursor solution was investigated. Precursor solutions containing $Al(NO_3)_3 \bullet 9H_2O$ and $LiNO_3$ in the ratios described in Scheme 3.1 were dried in the TGA as an isotherm for several hours at 90 °C. In the case of TGA analysis, a single drop of precursor solution was added to the dried powder after drying in an attempt to detect mass loss associated with solvent evaporation. DSC analysis was carried out on the dried powders without modification. Figure 3.1 shows the TGA analysis performed on the dried powders. The initial mass loss observed in the TGA occurring before 100 °C is attributed to dehydration of the damp precursor powder. Primary mass loss just beyond 100 °C accounts for roughly 60 percent of the total mass loss and is assigned to continuous dehydration of the powder and release of nitrates as the H_2O/HNO_3 azeotrope. Further mass loss occurs at a gradual rate with the TGA featureless up to 400 °C. As the DSC sample was dried for several hours prior to analysis, the absence of a corresponding endotherm with the primary mass loss observed in the TGA is expected. Simple nitrate salts are known to decompose over a wide range. Relevant to this system, pure aluminum nitrate decomposes at 170 °C while pure lithium nitrate decomposes at 640 °C.[80] The sharp endotherm located at 170 °C is consistent with the decomposition of a pure aluminum nitrate salt.[80] The sharp endotherm at 255 °C is consistent with the melting

temperature of $LiNO_3$. Between these sharp peaks, a broad endotherm begins just beyond 200 °C before being cut off at the 255 °C peak. This broad peak is within the range where simple nitrate salts are known to decompose and is likely the result of a nitrate salt mixture with an intermediate decomposition temperature with respect to the constituent salts. The endotherm located at 340 °C is attributed to residual nitrate decomposition as observed in similar systems.[103]

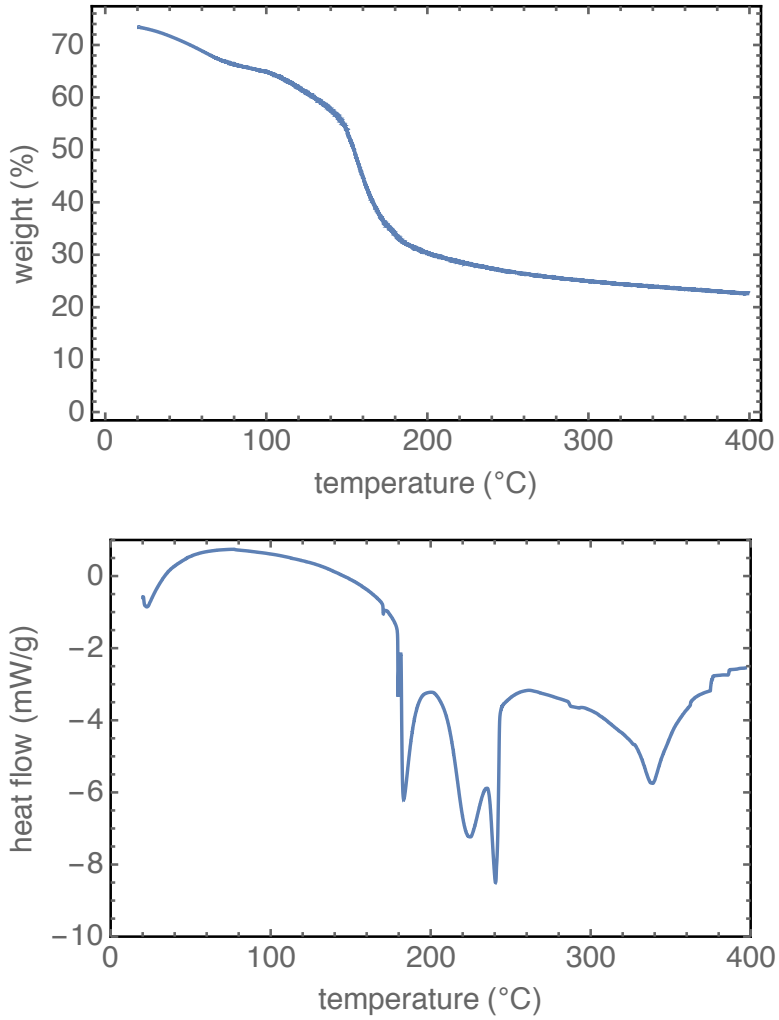

Figure 3.1. TGA and DSC curves of a LiAlO precursor powder from 20 to 400 °C.

The thermal data identified two temperatures of interest. The first is 275 °C, which is just beyond the endotherm peaks assigned to generic metal nitrate salt decomposition and/or melting points. The second temperature of interest is 400 °C, which is beyond any features observed in the TGA and DSC traces. Although thermal analysis was conducted on bulk powders, which are expected to behave differently than the pre-annealed, intimately mixed amorphous thin-film precursor, these two temperatures are expected to fully dehydrate films and decompose residual nitrates respectively.

Thin films were spun from precursor solutions with the same composition as that of those analyzed via TGA-DSC. Briefly, solutions were spun onto silicon substrates and immediately cured at 275 °C for 15 minutes. A final anneal at 400 °C under the flow of forming gas for one hour completed film fabrication. As the precursor materials are known to be hygroscopic, fabricated films were stored in desiccators prior to analysis to prevent the adsorption of water.

Single coat films were deposited as described above and analyzed via XRD (see Figure 3.2). Films are amorphous up to 400 °C. This result is expected as resistance to crystallization is common among metal oxide thin films prepared using PIC. The rapid film formation associated with PIC synthesis is necessary to prevent crystallization as observed with slow heating of precursor solutions.[42] Furthermore, crystallization of pure Al_2O_3 occurs at temperatures beyond those used in these experiments. Specifically, the initial stages of crystallization observed via *in-situ* low energy electron microscopy and diffraction begin between 450 °C and 500 °C.[105] Taken together the amorphous character of the LiAlO films is not surprising.

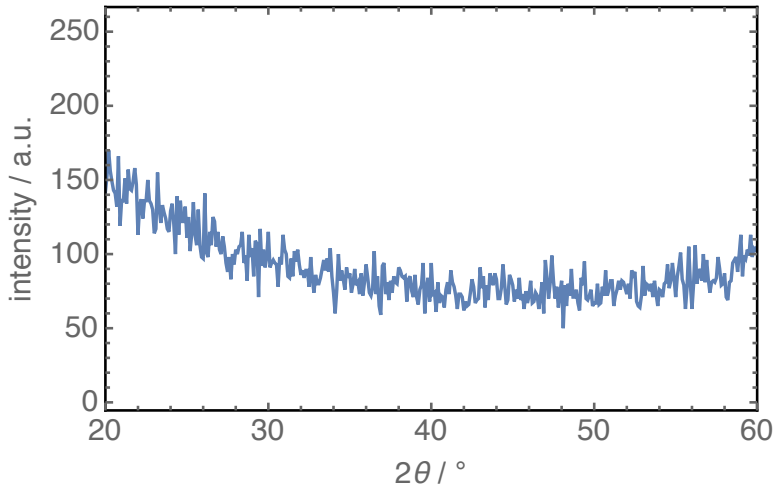

Figure 3.2. XRD of a LiAlO film annealed at 400 °C under forming gas for one hour.

FTIR spectra were collected to investigate the structure of the LiAlO films and monitor changes in film composition as a function of annealing temperature (see Figure 3.3). Absorption near 3600 cm^{-1}, indicative of hydroxyl stretching, was present in films annealed at 400 °C. The presence of hydroxyl groups are common to films prepared from aqueous solutions using PIC.[42] Additionally, the hygroscopic nature of the LiAlO films was observed throughout experimentation, and the presence of O-H stretches is not surprising. In the higher annealed sample, the broad peak at 3600 cm^{-1} gives way to a sharp peak centered at 3670 cm^{-1}. This peak is consistent with the presence of LiOH.[106] As with Al_2O_3, LiOH is hygroscopic, and the general broadness of the peak can be attributed to the presence of adsorbed water observed at 3574 cm^{-1}.[107] The absence of this peak at the higher annealing temperatures is expected as removal of O-H stretching associated with LiOH has been achieved through heating at 300 °C for 10-20 minutes.[101] Nitrate deformation vibrations are assigned to stretches in the 1200-1700 cm^{-1} range. These peaks are present in both annealing conditions indicating nitrate decomposition has not gone to completion by 400 °C. The presence of nitrates beyond 400 °C can be

explained when considering that the decomposition temperature of pure lithium nitrate is over 200 ^{o}C above the annealing conditions used in this study. Relative nitrogen content among samples of different annealing conditions was further investigated via XPS and is reported below. Absorptions in the 400-900 cm^{-1} range are representative of Al-O vibrational modes.[108]

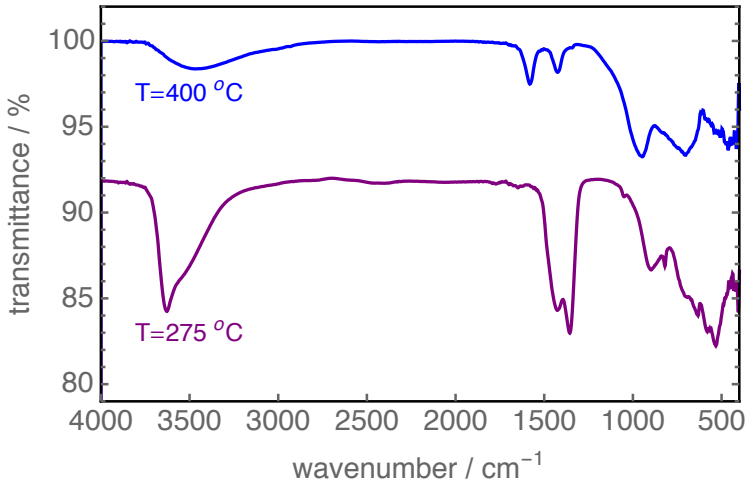

Figure 3.3. FTIR spectra of 110 nm LiAlO films annealed at 275 ^{o}C (purple) and 400 ^{o}C (blue) for one hour.

The surface composition of LiAlO thin films was determined by XPS. A survey scan detected the presence of Li, Al, O, C, and N (see Figure 3.4). The surface composition of the Li_2O-Al_2O_3 films is consistent with those reported in the literature.[100] For these measurements a surface composition of $Li_{0.8}Al_1O_z$ was obtained. XPS depth profiling demonstrated consistent atomic ratios as a function of depth. As observed in most air exposed samples, adventitious carbon was present with the C 1s peak located at 284.8 eV serving as a charge correction reference. A substantial decrease in carbon content was observed below the surface during depth profiling suggesting the carbon

source is likely atmospheric CO_2. The Li 1s peak at 55.1 eV is consistent with bulk Li and not that of LiOH (54.9 eV). The atomic ratio of aluminum to nitrogen is over 65:1 suggesting most residual nitrates have been decomposed by 400 ^{o}C. Furthermore, the N 1s peak associated with nitrates (407.3 eV) is absent from the scan. This reduced nitrogen content is consistent with a reduction in the intensity of the nitrate stretch for the higher annealed films as observed by IR. The O 1s peak is consistent with Al-O bonding found in Al_2O_3 (531.0 eV) with no evidence of Al-OH (532.1 eV). Further support for the absence of Al-OH is found in the Al 2p spectra where there is a lack of binding energies associated with Al-OH (74.2 eV). The Al 2p peak is located at 74 eV and consistent with Al_2O_3. Taken together the aluminum appears to be fully oxidized in an Al-O-Al network. Finally, it should be noted that the O 1s peak had a minor contribution from oxygen associated with H_2O (532.8 eV). As previously mentioned this small amount of water is expected as the LiAlO thin films are hygroscopic.

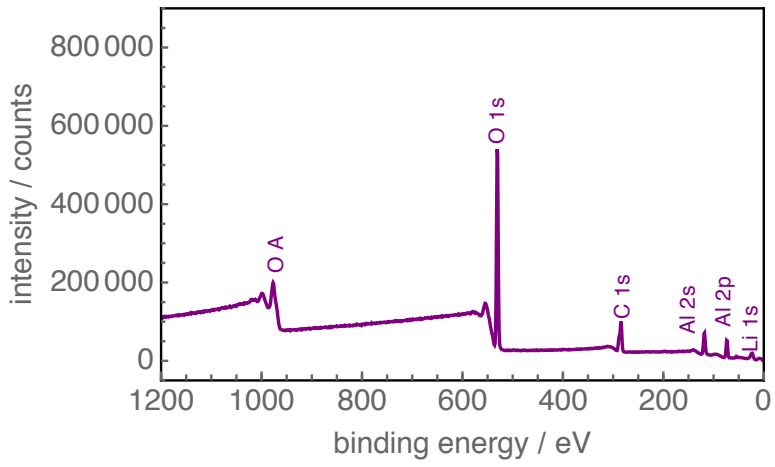

Figure 3.4. Survey scan of LiAlO films annealed at 400 ^{o}C for one hour.

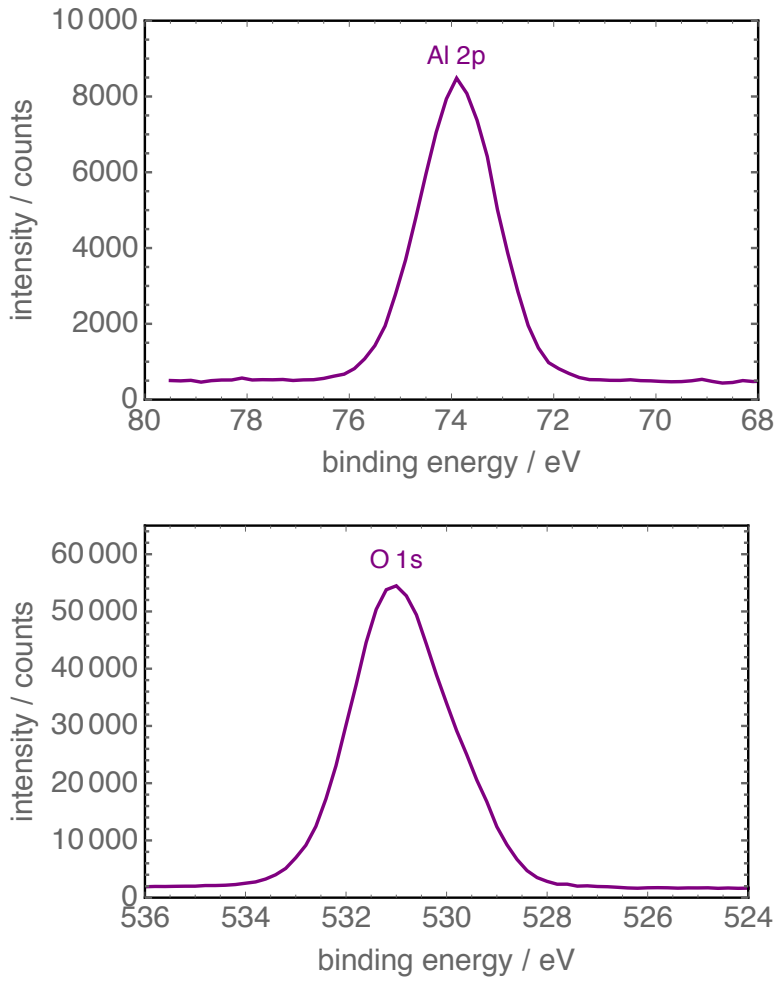

Figure 3.5. Al 2p and O 1s peak for LiAlO films annealed at 400 ^{o}C for one hour.

LiAlO films were imaged using scanning electron microscopy (SEM) to determine morphology (see Figure 3.6). Thin-film oxides prepared using PIC routinely produce quality films as defined by high density and smoothness, in addition to low porosity. This quality is observed herein further establishing PIC synthesis as an effective synthetic method to the production of exceptional thin films. Furthermore, obvious signs of cracking are absent in LiAlO thin films despite rapid dehydration and counterion elimination. As previously reported, this suggests the formation of the solid-state thin

films from aqueous solutions is a relatively forgiving transition generating low levels of film stress.[103]

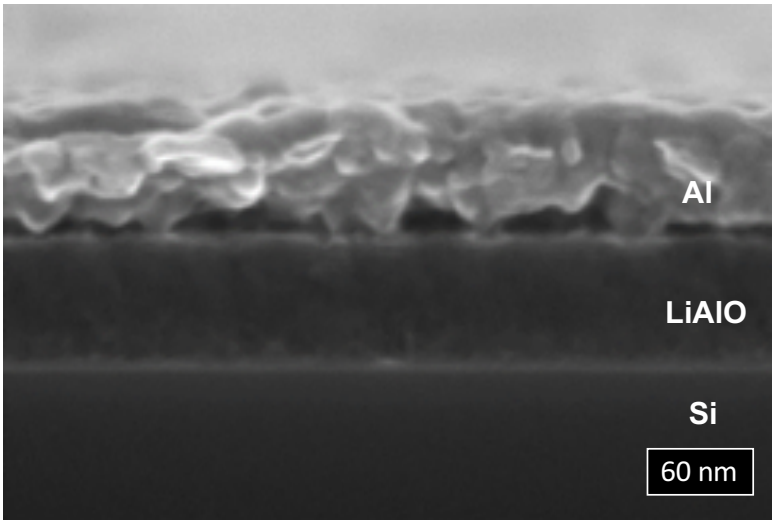

Figure 3.6. Cross-sectional SEM of 70 nm LiAlO film annealed at 400 ^{o}C for one hour.

Thin-film thickness can be tightly controlled via precursor concentration (see Figure 3.7). In this work, single layer thin films were fabricated between 13 nm and 58 nm corresponding to concentrations ranging from 0.1 M to 0.5 M. This near linear relationship between precursor concentration and film thickness using PIC has been demonstrated in previous studies.[43,103] Furthermore, multiple layers of the same concentration of precursor solution can be used to achieve desired thicknesses outside of the reported range for single layer films. These multi-layer films appear as a single layer when imaged via SEM.

Impedance spectroscopy was used for the electrical characterization of LiAlO thin films. The real part of the apparent permittivity as a function of frequency is presented in Figure 3.8. These measurements yield a low frequency ε'_{app}= 600 for an 81 nm thick film. The large magnitude of ε'_{app} is common to ion conducting thin film oxides and is

attributed to polarization of ions against the ion-blocking electrode. As expected, this low frequency ε'_{app} is dependent on thickness as the governing property determining the dimension of the ionic double layer is the Debye length of the electrolyte, a material property independent of film thickness. Considering the capacitance at low frequency associated with the ionic double layer is near constant and independent of thickness, representation of the ε'_{app} at the same frequencies will be thickness dependent.

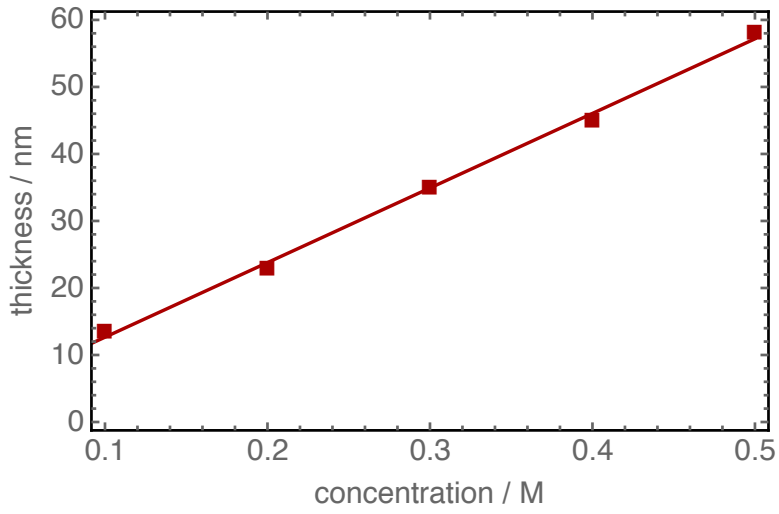

Figure 3.7. LiAlO film thickness as a function of precursor concentration annealed at 400 ^{o}C for one hour.

Conversely, the high frequency side of the plot represents an ε'_{app} value that is independent for thickness and for LiAlO samples, a value of $\varepsilon'_{app} = 5$ is obtained. For comparison, literature values for lithium aluminum oxide prepared via high temperature (1500 °C) melt quenching techniques have a high frequency value of $\varepsilon'_{app} = 5.3$.[109] These values are in good agreement with one another despite the large differences in synthetic methods and LiAlO material form. In addition to deviations in preparation, the reported

literature values of ε'_{app} are for bulk powders while those presented in this work are for thin films.

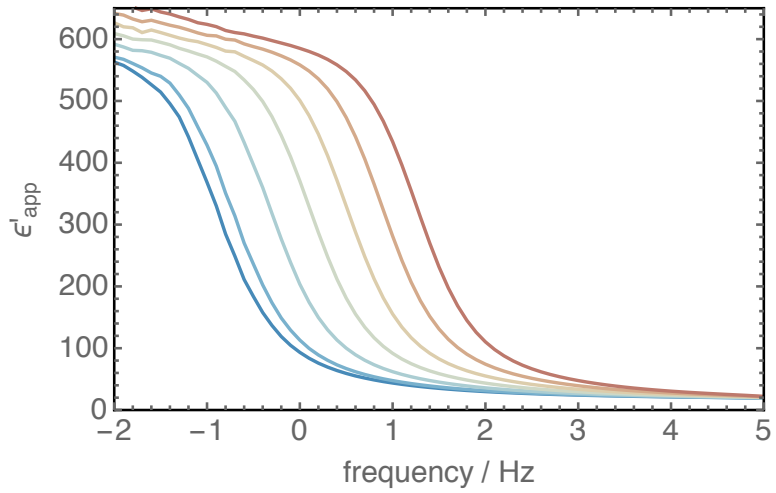

Figure 3.8. Frequency dependent real part of the apparent permittivity (ε'_{app}) as a function of temperature over the range 30 °C to 90 °C in 10 °C increments for an 81 nm thick LiAlO film annealed at 400 °C for one hour.

Incorporation of monovalent alkali metals is known to increase capacitance values.[7,85,87] This phenomenon is attributed to the electric double layer related to ion polarization against blocking electrodes.[110,111] As previously reported, lithium incorporated alumina saw an increase in observed capacitance over that of plain alumina, increasing from 0.1 μF cm^{-2} to 0.2 μF cm^{-2} when measured at 100 Hz and 100 °C. For the same frequency and temperature, LiAlO films in this study had a capacitance of 2.9 μF cm^{-2} (see Figure 3.9). A possible explanation for these discrepancies is sample storage and care. The authors mention that capacitance values drop upon aging citing lithium incorporated alumina as most severely affected. The authors also suggest levelling of the capacitance values at low frequency but did not investigate capacitances below 100 Hz. Measurements presented in this study were carried out to 10 mHZ and the levelling suggested by Liu et al. is confirmed with capacitance values surpassing 6 μF cm^{-2}. The

large capacitance values and associated decrease in operating voltage for devices incorporating materials like those synthesized in this study have led to recent interest for their use as gate dielectrics in field-effect transistors.[7,85] The results presented herein indicate LiAlO films synthesized by PIC are promising material for this particular function.

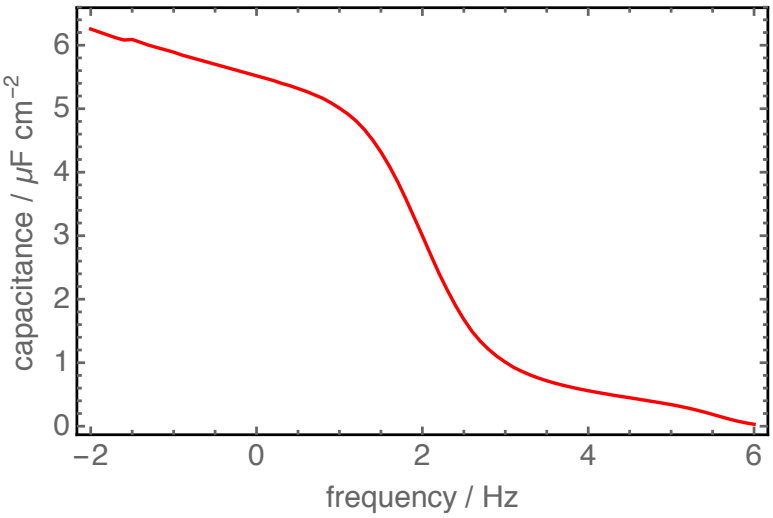

Figure 3.9. Capacitance as a function of frequency of a LiAlO film measured over a frequency range of 1 MHz to 10 mHz.

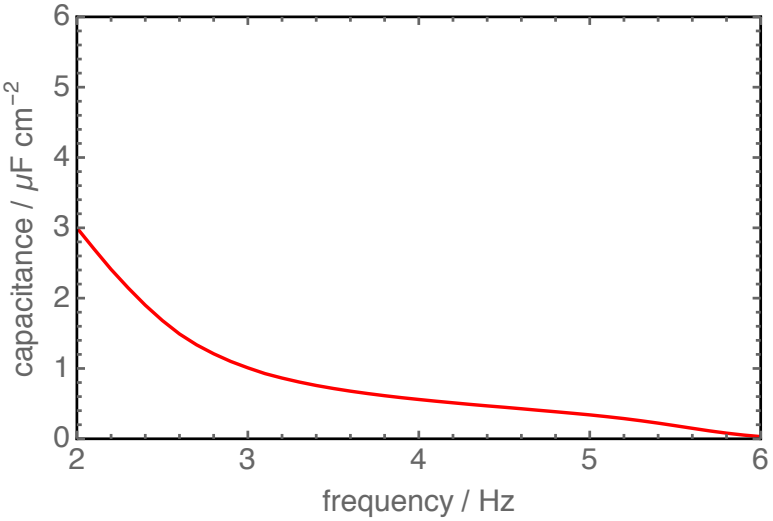

Figure 3.10. Capacitance as a function of frequency of a LiAlO film measured over a frequency range of 1 MHz to 100 Hz.

A plot of the real part of the apparent conductivity, σ'_{app}, as a function of frequency yields a plateau region assigned to the bulk resistance of the solid electrolyte (see Figure 3.11). From this resistance, the DC ionic conductivity of the film can be determined. As previously mentioned, determination of this conductivity value is complicated by the low frequency drop in σ'_{app} due to ion polarization and the possibility that the ionic conductivity is inherently frequency dependant.[83] These factors make it difficult to extrapolate the ionic conductivity contribution of σ'_{app} to its DC value. One approach to estimate the DC ionic conductivity is to use the dielectric loss. Specifically, the peak in the dielectric loss and its associated frequency provides a consistent point in the conductivity plot from which the DC ionic conductivity can be estimated.[84,103] This estimate has been found to be consistent with more complete equivalent circuit modelling of the ionic conductivity data. The DC conductivity of LiAlO films was determined to be $\sigma_{DC} = 8.8 \times 10^{-8}$ S cm^{-1}, analogous to LiAlO prepared via expensive vacuum deposition and annealed at high temperature.[100] Additionally, these literature reported values for LiAlO conductivity are typically reported for measurements collected in excess of 300 ^{o}C. Extrapolation of this data is then used for commentary on room temperature conductivities. Although the use of extrapolated data from other studies allows for a direct comparison to the calculated conductivities presented herein, it should be noted that conductivity does not necessarily track linearly with temperature, especially within lower temperature regimes. Despite the potential for deviations from linearity, the presented data compares favourably to extrapolated conductivities reported in other studies.[100]

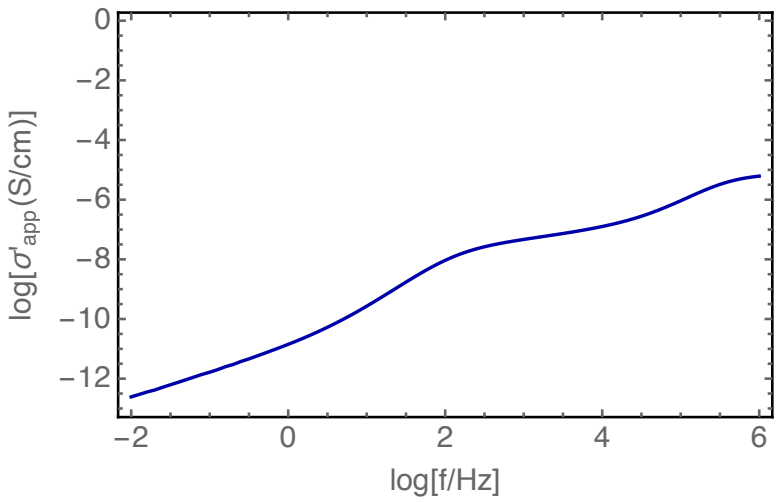

Figure 3.11. The real part of apparent conductivity σ'_{app} (blue line) as a function of frequency measured at 100 °C of a 81 nm thick LiAlO film annealed at 400 °C for one hour.

Activation energies were determined by plotting log σ_{DC} versus $1/T$ according to the Arrhenius equation: $\sigma = A \exp[-E_a/(kT)]$ where A is the pre-exponential factor, E_a is the activation energy, k is the Boltzmann constant, and T is temperature (see Figure 3.12). The value of E_a extracted from the linear fit of the log σ_{DC} versus $1/T$ is 0.81 eV. This value is consistent with the activation energies reported for non-crystalline LiAlO reported by Glass et al.[10] Analogous activation energies suggest a similar mechanism of ionic conduction. Furthermore, this similarity in E_a supports the proposal that lithium is the mobile ion species responsible for the observed conductivity within the LiAlO network. This similarity is particularly important with aqueous solution deposited films, where incomplete dehydration can result in measured proton conductivity, resulting in an inaccurate description of the conductivity associated with the synthesized lithium ion conductor.

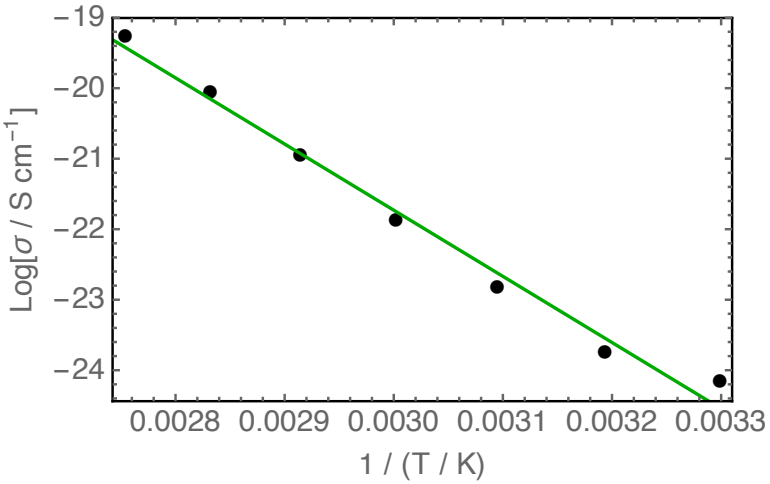

Figure 3.12. Arrhenius plot of the DC conductivity σ_{DC} value at the peak in the loss tangent, tan δ, frequency from 81 nm thick LiAlO films annealed at 400 °C.

Conclusions

We have reported the synthesis of amorphous LiAlO thin-films deposited from aqueous solutions using PIC chemistries. The measured lithium ion conductivity is σ_{DC} = 8.8 x 10^{-8} S cm^{-1}, consistent with those values reported in the literature. An activation energy of E_a = 0.81 eV was obtained, analogous to glassy LiAlO prepared via energy intensive processing. Films deposited from homogenous solutions produced pinhole free films over the thickness range of 13 nm to 110 nm. This study represents a sustainable approach to the production of the ISE LiAlO, utilizing low temperature processing. Additionally, the large double layer capacitance and theoretical reduction in transistor device operating voltage suggest these films may be of interest as gate dielectrics in field-effect transistors. Furthermore, the high quality of films defined by high density, smoothness, and low porosity suggest that LiAlO thin films are excellent candidates for layered systems including nanolaminates for the purpose of tuning of material properties.

Bridge

Chapters II and III have demonstrated the use of PIC chemistry to produce inorganic solid-state electrolytes in thin-film form. Chapter IV will demonstrate the incorporation of the ionic conductor LiAlO, described in this chapter, into more complex structures. Specifically, the ionically conductive LiAlO will be layered with non-conductive TiO_2 and characterized as a function of structure. This work will provide insight into the properties that influence film quality in solution deposited multi-layered nanolaminates in addition to a description of the resultant electrical performance of these materials.

CHAPTER IV

ROLE OF NANOSTRUCTURE IN NANOLAMINATE STACKS SYNTHESIZED FROM AQUEOUS PRECURSOR SOLUTIONS

This chapter contains previously unpublished and co-authored material. Experimental work and writing was done primarily by me. K. Woods assisted in the collection of microscope imaging. M. Lonergan provided editorial assistance.

Introduction

Thin-film metal oxides are a useful class of materials common to several electrochemical systems. A large body of research has focused on the synthesis and characterization of oxides with high relative permittivity (ε_r).[112] As with any class of materials, maximizing useful properties while minimizing undesirable qualities is a primary goal. A major step toward the improvement of metal oxides used as dielectrics was the incorporation of dopants to reduce adverse characteristics including high leakage currents.[113] Although this method is effective for improving the performance of bulk materials, it is limited with respect to the range over which material properties can be controlled. A significant advancement in this area of research, specifically addressing this issue, came in the form of nanolaminates, which use alternating materials in multi-layered stacks. A major advantage of these systems is that the nanolaminate stack often merges positive characteristics of each layer into one enhanced material. The result of this merger is that many materials exhibit superior physical and/or electrical properties when compared to that of the constituent layers.[61,64]

Although multi-layered structures have received considerable interest over recent years, there is room for expansion with respect to constituent layer identity. Of particular interest, with respect to the tuning of material properties, is the use of alkali metal ion incorporated metal-oxide films. Polarization of conductive ions against blocking electrodes yields large values of the apparent dielectric constant, ε'_{app}. The use of these ion incorporated metal-oxide films in electrochemical systems has been previously established with alkali metal incorporated aluminum oxide specifically identified as possessing superior performance, showing a substantial decrease in device operating voltages.[7,85,87] As alkali metal ion-incorporated metal-oxide films possess excellent physical properties, including high apparent dielectric constants, they are promising for use in layered systems. Interspersing ionic conductors with non-ionic conductors in nanolaminates, creates new structures where the distances over which ions polarize are controlled by the laminate structure. The prospect for large spatial displacements will mimic the large ionic displacements observed in high dielectric single phase materials, but with the added benefit of direct control over layer thickness and thus, dielectric constant.[114] In addition to the tuning of dielectric constant, the use of nanolaminate architecture is expected to have a positive affect on the voltage stability compared to single-phase materials. This is because the voltage will be dropped across several double layers rather than the lone layer found in a single-phase material.

The synthesis of multi-layered nanostructures has been dominated by atomic layer deposition and magnetron sputtering.[53] Although quality films can be prepared by these methods, an alternative, low cost, low energy, environmentally friendly synthetic method is of great interest. The use of prompt inorganic condensation (PIC) has been established

as an effective method for the deposition of quality metal oxides.[42,47,50] PIC has also been used for the deposition of high quality thin film ionic conductors.[103] Furthermore, PIC can also be utilized for fabrication of nanolaminate structures.[46,74] Collectively, PIC is a valuable tool for the synthesis of high quality nanolaminates, which include constituent layers that are ionically conductive, thus creating new structures with unique characteristics. Furthermore, structures will be synthesized using a low energy, environmentally benign synthetic method.

We have reported herein the synthesis of nanolaminates composed of alternating layers of the ionically conductive Li_2O-Al_2O_3 with non-conductive TiO_2. High quality films of both constituent layers have been successfully deposited via PIC. Li_2O-Al_2O_3 is known to have high thickness dependent apparent ε' and therefore provides opportunity for the tuning of dielectric constant. TiO_2 also has high dielectric constant values but is limited by the high leakage currents associated with its crystalline form. This study aims to demonstrate improved electrical characteristics of layered materials over their single-phase predecessors. Here we demonstrate that PIC can be utilized as a low energy approach to the production of quality nanolaminates with high levels of smoothness, uniformity, and layer integrity.

Experimental

Precursor Synthesis

The LiAlO precursor solution was prepared as previously reported. $Al(NO_3)_3 \bullet 9H_2O$ (Alfa Aesar) and $LiNO_3$ (Alfa Aesar) were dissolved in 18 MΩ H_2O, combined and allowed to stir overnight at room temperature. The solution was diluted

with 18 MΩ H_2O to achieve desired concentrations with a maximum value of 0.5 M with respect to Al. The Al:Li ratio was 1:1 for all precursor solutions. The TiO_2 solution was prepared as follows: $TiOSO_4 \cdot xH_2O + H_2SO_4$ was dissolved in 18 MΩ H_2O and allowed to stir at room temperature overnight. The clear solution was diluted with 18 MΩ H_2O to 0.64 M. A 15 percent (w/v) NH_3 (aq) (Sigma Aldrich) solution was added dropwise to the clear solution until pH = 7. The resultant precipitate was centrifuged and washed (5x). The white precipitate was dissolved in H_2O_2 (aq) (29.0-32.0 % EMD Millipore) over ice until the orange solution had a pH = 3. Dropwise addition of 15 percent (w/v) NH_3 (aq) (Sigma Aldrich) was completed until pH = 10. The yellow precursor solution was kept over ice and stable for approximately 48 hours.

Film Deposition and Device Fabrication

Films were prepared by solution deposition of single layer films via spin-processing. Boron doped Si substrates (0.008-0.020 Ω cm) were sonicated in a five percent Contrad 70 solution for 60 min at 50 °C. Substrates were then treated by plasma cleaning to produce a hydrophilic surface (120 s O_2/N_2 plasma etch using a Plasma Etch, Inc. PE-50 Benchtop Plasma Cleaner set to maximum power). The precursor solution was filtered (2x) through a 0.45 μm Teflon filter. Substrates were flooded with filtered precursor solution via syringe and spun at 3000 rpm for 30 s. An immediate hot plate cure at 275 °C was carried out for fifteen minutes. This spinning and curing process was repeated with alternating LiAlO and TiO_2 precursor solutions to achieve desired nanolaminate architecture. A final anneal at 400 °C was then carried out for one hour under the flow of forming gas. An array of circular (0.011 cm^2) Au top contacts was

thermally evaporated onto the film surface via shadow mask. An Al plate adhered by silver print to the silicon wafer was used for a back contact.

Characterization

X-ray reflectivity and diffraction measurements on thin-film samples were collected on a Bruker AXS D8 Discover diffractometer with Cu Kα radiation to determine the total film thickness. The chemical characteristics of films were investigated by X-ray photoelectron spectroscopy (Thermo Scientific ESCALAB 250 X-ray Photoelectron Spectrometer). All binding energies were referenced to the C 1s peak of carbon at 284.8 eV. NIST and LaSurface XPS databases were used for binding energy assignments. Film morphology and thickness were characterized using a ZEISS Ultra-55 Scanning Electron Microscope. Impedance spectroscopy measurements were performed using a Solartron 1260 Impedance Analyzer and 1296 Dielectric Interface over the frequency range 10 mHz to 1 MHz. Temperature control was achieved using a Sun Electronic Systems Environmental Chamber (Model EC1X). The apparent relative permittivity $\varepsilon_{app} = \varepsilon'_{app} - i\varepsilon''_{app}$ and conductivity $\sigma_{app} = \sigma'_{app} + i\sigma''_{app}$ were calculated from the raw complex impedance Z in the standard manner: $\varepsilon_{app} = \sigma_{app}/i\omega\varepsilon_0 = L/i\omega AZ\varepsilon_0$ where ε_0 is the vacuum permittivity. The dielectric loss tangent $\tan\delta = \varepsilon''_{app} / \varepsilon'_{app} = \tan(\theta + \pi/2)$, where θ is the measured phase angle (radians), was also calculated. Breakdown voltage measurements were done on a Keithley 236 source measurement unit with a scan rate of 10 mV s^{-1}.

Results and Discussion

PIC synthesis was utilized to deposit alternating layers of LiAlO and TiO_2 in several nanolaminate structures. The individual layers were spin deposited from stock solutions appropriately diluted for desired thicknesses. A hot plate anneal at 275 °C for 15 minutes took place following each deposition to lock-in the thin-film structure, effectively rendering the deposited layer insoluble during subsequent depositions. Following the final deposition of the last constituent layer, a final furnace anneal at 400 °C completed the laminate structure.

As previously reported, PIC synthesis produces high quality films of LiAlO over a wide thickness range that can be tightly controlled. Dilution of stock solutions allowed precise control over constituent layer thickness. As with the LiAlO system, TiO_2 precursor concentration tracks linearly with film thickness (see Figure 4.1). Film thicknesses were determined via ellipsometry and confirmed via x-ray reflectivity.

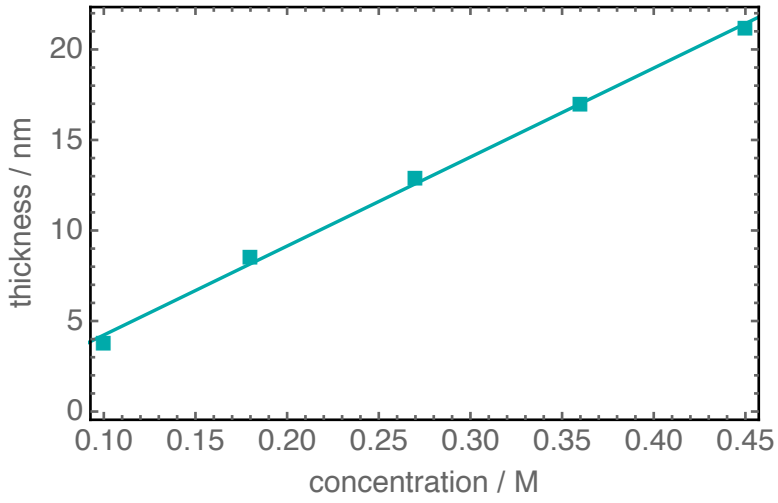

Figure 4.1. TiO_2 film thickness as a function of precursor concentration. Films were annealed at 400 ^{o}C for one hour.

Surface composition of TiO_2 layers was determined via XPS. A survey scan detected the presence of Ti, O, Si and C (see Figure 4.2). The observed surface atomic percentages are consistent with TiO_2, with a slight oxygen enrichment attributed to atmospheric oxygen. As with other air-exposed samples, carbon content decreased as a function of film depth. This decrease is expected as the primary source of carbon is attributed to atmospheric CO_2, which is not known to penetrate beyond the first few nanometers of the film. Titanium presence was observed throughout the film during depth profiling at atomic percentages suggesting an even distribution of titanium within the film. This even distribution is important; as atomic enrichment of particular elements can occur during film fabrication. The binding energy of the Ti 2p peak located at 458 eV is characteristic of TiO_2 (see Figure 4.3). Additionally, the O 1s oxygen peak is at a binding energy (529.8 eV) typical of oxygen in TiO_2 (see Figure 4.3). Surface analysis of LiAlO films yielded atomic percentages of Li, Al, and O that are representative of the precursor solution. The obtained percentages are consistent with values acquired for LiAlO films previously synthesized (Chapter III). All associated binding energies for individual elements are characteristic of Li_2O-Al_2O_3.

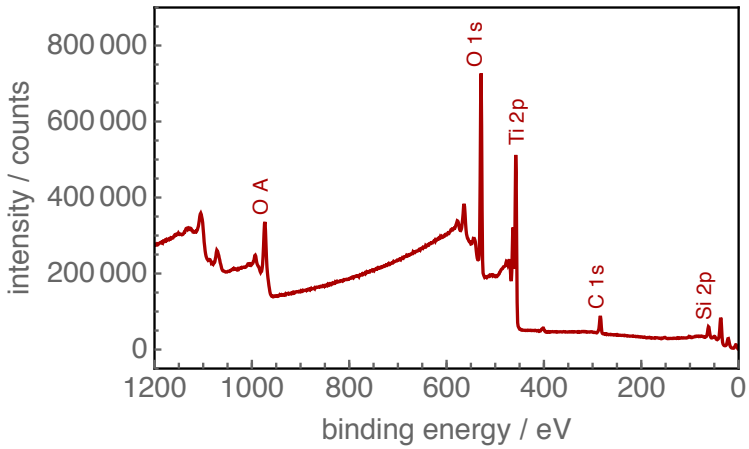

Figure 4.2. Survey scan of TiO_2 films annealed at 400 ^oC for one hour.

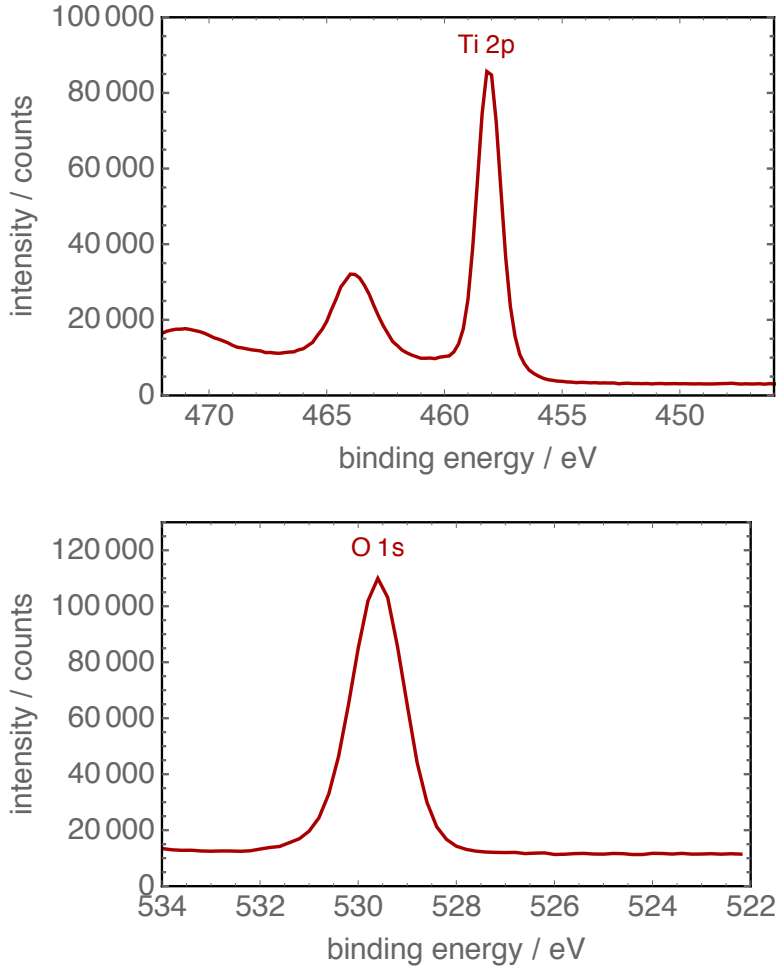

Figure 4.3. Ti 2p and O 1s XPS scans for TiO_2 films annealed at 400 ^oC for one hour.

Single layers of LiAlO and TiO_2 deposited via PIC were investigated by XRD. LiAlO films were determined to be amorphous while TiO_2 exhibited diffraction peaks representative of the anatase phase of crystalline TiO_2 (see Figure 4.4). The amorphous nature of the LiAlO layer is consistent with previous studies on aqueous solution deposited LiAlO (Chapter III). Crystallinity is common to TiO_2 films annealed at temperatures as low as 250 ^oC and is therefore expected for films annealed at 400 ^oC.[73]

Alternating layers of LiAlO and TiO_2 were deposited from aqueous precursors as described above. Briefly, TiO_2 was deposited onto cleaned substrates and immediately cured at 275 ^oC for 15 minutes. A layer of LiAlO was then deposited onto the freshly annealed TiO_2 film and exposed to the same heat treatment. This process was repeated resulting in a nanolaminate stack with a total of five individual layers, which was then annealed at 400 ^oC for one hour. Nanolaminate films were analyzed by XRD and are presented in Figure 4.5. In contrast to single layer TiO_2, the TiO_2: LiAlO stacks appear amorphous when annealed at 400 ^oC for one hour. When samples are heated at the same temperature for an extended period (18 hours) peaks indicative of crystalline TiO_2 in the anatase phase emerge. This resistance to crystallization observed in nanolaminate structures has been observed in other systems.[74]

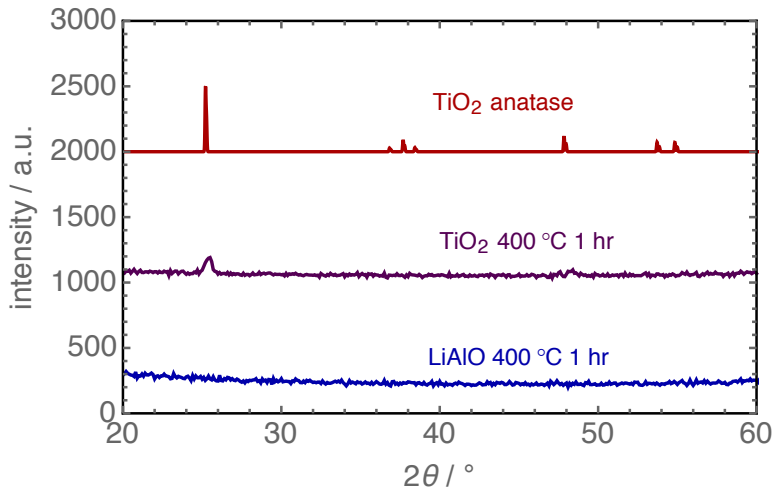

Figure 4.4. XRD of single layer LiAlO (blue) and TiO_2 (purple) films annealed at 400 ^oC for one hour. A TiO_2 standard (anatase) is included for reference (red).

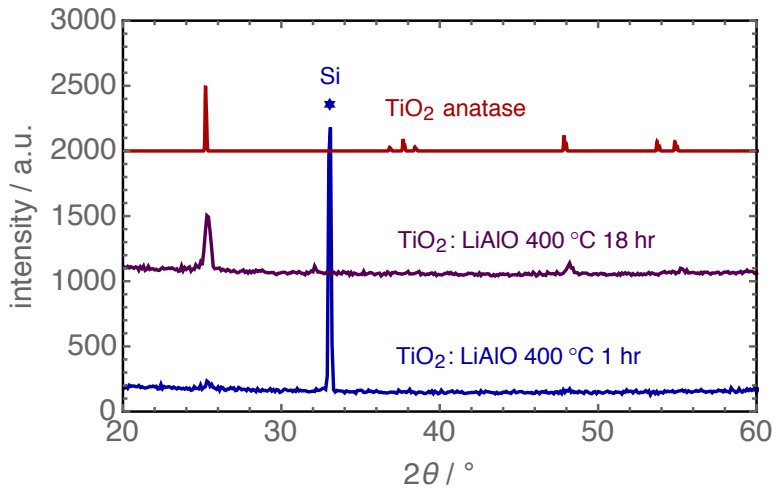

Figure 4.5. XRD of five-layer TiO_2:LiAlO nanolaminate stacks annealed at 400 ^oC for one hour (blue) and 18 hours (purple). A TiO_2 standard (anatase) is included for reference (red).

XRR patterns display resolvable Kessig fringes to relatively high 2θ values (see Figure 4.6). The smoothness and parallel nature of the interfaces is described by the Parratt relationship: $\Delta t = \frac{\lambda}{4(\theta_i^2 - \theta_c^2)^{\frac{1}{2}}}$, where Δt is the film roughness, λ is the wavelength, θ_i is the angle at which films are no longer resolvable, and θ_c is the critical angle.[115] The pattern shown in Figure 4.6, demonstrates a θ_i value of approximately 6°, indicative of highly smooth and parallel interfaces. Irregular peak intensity results from the interference of the multilayer stack. The pseudo-periodic variation in electron density in the film, which could be expected to result in diffraction intensity, adds additional complexity.[116] In a traditional superlattice film, the number of Kessig fringes between Bragg maxima can often be used to detect the number of bilayers in a film when integer unit cell numbers are present. Because a total of five layers representing a unit cell number equalling 2.5 were deposited, the small and non-integer number of bilayers makes interpretation of the pattern challenging.

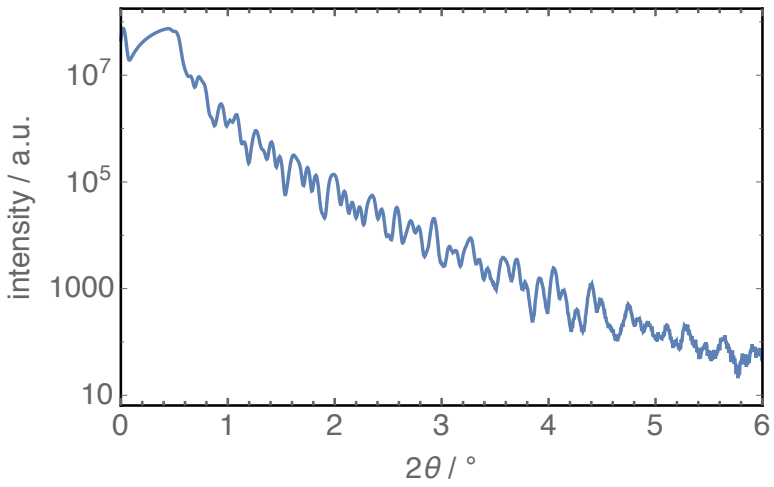

Figure 4.6. XXR scan of five-layer TiO_2:LiAlO nanolaminate stack annealed at 400 ^oC for one hour.

The five layer nanolaminate stack was imaged via cross-sectional SEM (see Figure 4.7). Aluminum was thermally evaporated on top of the stack to aid in focusing of the electron beam. Constituent layers of LiAlO and TiO_2 appear dense with clearly defined interfaces. In agreement with the diffraction data, LiAlO layers appear amorphous. Interestingly, TiO_2 layers appear to have crystallized with distinct grains. Careful inspection of the XRD pattern for the same sample, annealed at 400 ^oC for one hour, reveals the emergence of a diffraction peak located near 25°, rising just beyond the noise. This peak is representative of crystalline TiO_2 (anatase). Despite the high volume loss associated with the PIC process, the stack is free of cracking and large voids. Additionally, individual layers appear discrete with no intermixing or delamination of the stack. The total film thickness equals approximately 118 ± 2 nm, which is consistent with thickness values obtained via ellipsometry for single films of constituent layers. Individual layers of TiO_2 have consistent thickness values that are in good agreement

with one another (25.6 nm, 27.7 nm, and 26.3 nm). A larger deviation exists between the two LiAlO layers (22.6 nm and 16.5 nm). As previously demonstrated LiAlO and TiO_2 thickness track linearly with precursor concentration. As all layers of LiAlO were deposited from the same precursor concentration, it was expected that individual layers would be of the same thickness, which was not observed. Small deviations in thickness can likely be attributed to variation in the relative humidity of the spin coater chamber, which was not controlled for.[51]

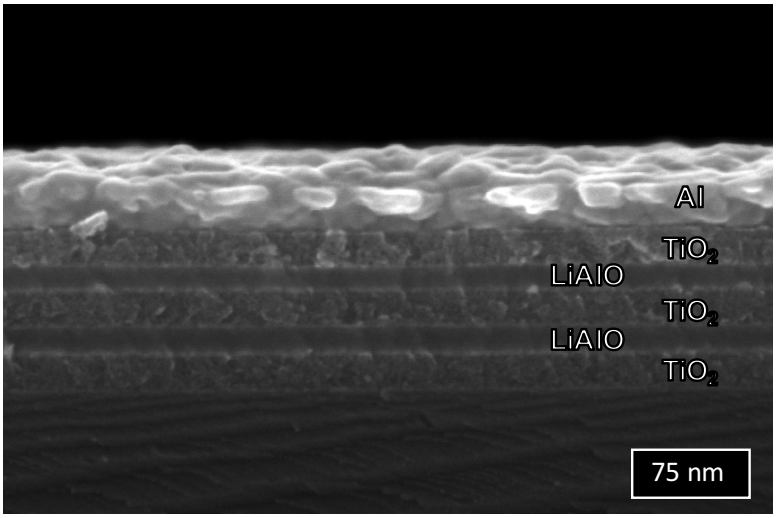

Figure 4.7. Cross-sectional SEM of a five-layer stack of TiO_2 and LiAlO deposited on a silicon substrate and annealed at 400 ^{o}C for one hour.

A secondary explanation for observed disparities is the differences in wetting characteristics of LiAlO layers in subsequent depositions. Following the initial cleaning process, silicon substrates are plasma cleaned to generate a hydrophilic surface for the deposition of aqueous solutions of LiAlO. When depositing single layer films, the solution is deposited onto the freshly cleaned, hydrophilic surface and has excellent wetting characteristics. A change in these characteristics is observed upon successive

depositions required in multi-layered systems, with observable inconsistencies in the surface flooding behaviour. Additionally, the surface roughness of the substrate is changed following a deposition of a thin film layer. Despite the high level of smoothness associated with PIC deposited films, it is impossible to replicate the quality of bare silicon. As layers are continually deposited, the surface topography becomes unique to the previously deposited layer. Any deviations at the surface of the film are propagated throughout the stack. Taken together, it is not unexpected that films deposited early in the nanolaminate sequence exhibit qualities, particularly thickness, most consistent with that of single films from equivalent precursor solutions. The fact that each layer appears discrete with no major film disruptions speaks volume to the quality of the PIC method.

Surface crusts, or regions of higher film density, have been observed in PIC deposited films suggesting a small amount of film inhomogeneity, particularly at the surface of each layer.[117] Fairley et al note several factors that can affect the presence and characteristics of these crusts, including annealing temperature, ramp rate, humidity, and metal oxide identity. The idea that the identity of the metal oxide plays an important role in PIC films has been demonstrated by Jiang et al.[74] In this study, alternating layers of TiO_2 and $Al_4O_3(PO_4)_2$ were deposited in nanolaminate structures. The resident layers had remarkably different responses to annealing temperatures with respect to changes in film density and thickness. These differences were attributed to water content disparities between the $Al_4O_3(PO_4)_2$ and TiO_2 layers, which may explain the increased agreeability of thickness among TiO_2 layers in the nanolaminate stack presented herein. The consistency of the TiO_2 thickness along with previous studies commenting on uniformity with respect to density suggest that TiO_2 films spun from aqueous solution are more

robust than those of LiAlO. Furthermore, it should be noted that the presence of dense sections of the films, particularly near the surface, may provide a barrier against re-dissolution of previously deposited layers. This protective barrier is likely a contributing factor to the integrity of the layer interface observed via SEM. At this time there is no evidence of crust formation in this system. More importantly there is no observed composition inhomogeneity within the films as determined via XPS which covers the full depth of the surface crust described by Fairley et al.[117]

To ascertain the role of nanostructure in laminate stacks, samples of variable constituent thickness were deposited on cleaned silicon substrates as described above (see Figure 4.8, 4.9, and 4.10). A major goal of this work was to manipulate laminate structure while retaining total film thickness across multiple samples. This effort was to ensure that changes in observed laminate behaviour could not simply be attributed to variable film thickness and instead must be explained by variations in nanostructure. For this study, three laminate structures were proposed. All three types of laminates have the same three layer LiAlO:TiO_2:LiAlO stack scheme. The major difference in film design is the thickness of the central TiO_2 layer. The observed thicknesses of these TiO_2 layers as assessed via SEM imaging were ~ 7 nm, ~ 13 nm, and ~ 27 nm, referred to hereafter as thin, medium and thick TiO_2 respectively. Stock solution of TiO_2 was diluted as appropriate, utilizing the aforementioned concentration versus thickness curve (see Figure 4.1), to achieve these thicknesses. These results are in remarkable agreement with the proposed thicknesses during initial laminate design. To maintain a constant total film thickness, LiAlO layers were diluted in the same manner as the TiO_2 layers described above. As with the TiO_2 layers, individual LiAlO layers tracked appropriately with the

concentration versus thickness curve of LiAlO (Chapter III). The average total thicknesses of the three film types via ellipsometry were measured to be 41.9 nm, 39.4 nm, and 42.5 nm. The resultant total film thicknesses are in outstanding agreement with the intended target thickness and demonstrate the high level of control PIC synthesis offers for complex, multi-layered structures. These thickness values were determined from the ellipsometry data using the model described by Mitchell et al., where individual layer thickness of a multilayer stack was allowed to vary.[118] In their study, Mitchell et al. found that ellipsometry data for a modelled three layer stack of Al_2O_3:TiO_2 was only ± 1.6 nm when benchmarked against TEM.[118] In the present study, thickness data obtained via ellipsometry is in good agreement with SEM data with respect to total film thickness. Additionally, SEM images demonstrate that the experimentally obtained constituent layer thicknesses and total film thicknesses are consistent over the length of the film with no major deviation from the proposed thicknesses during pre-experimental laminate design.

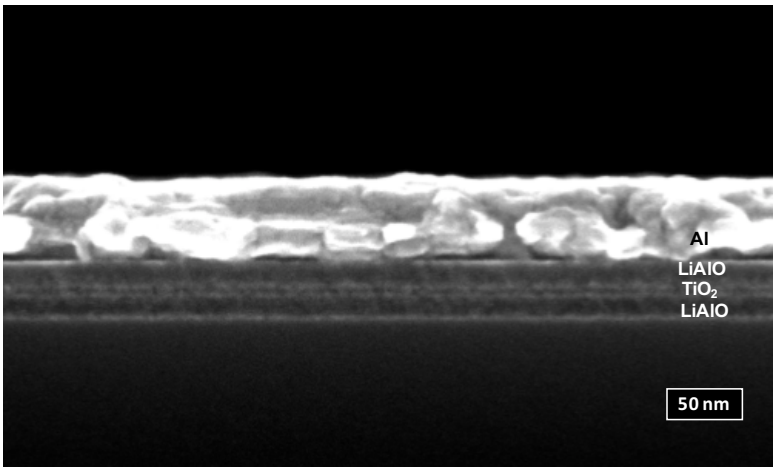

Figure 4.8. Cross-sectional SEM of the thin TiO_2:LiAlO three-layer stack deposited on silicon and annealed at 400 ^oC for one hour.

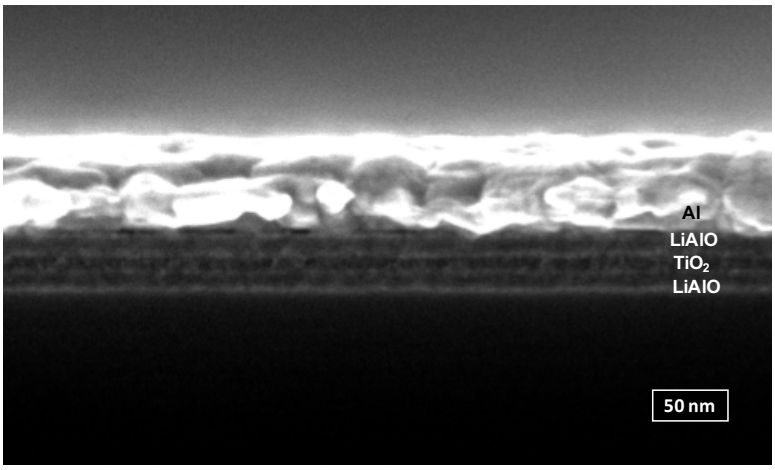

Figure 4.9. Cross-sectional SEM of the medium TiO_2:LiAlO three-layer stack deposited on silicon and annealed at 400 ^oC for one hour.

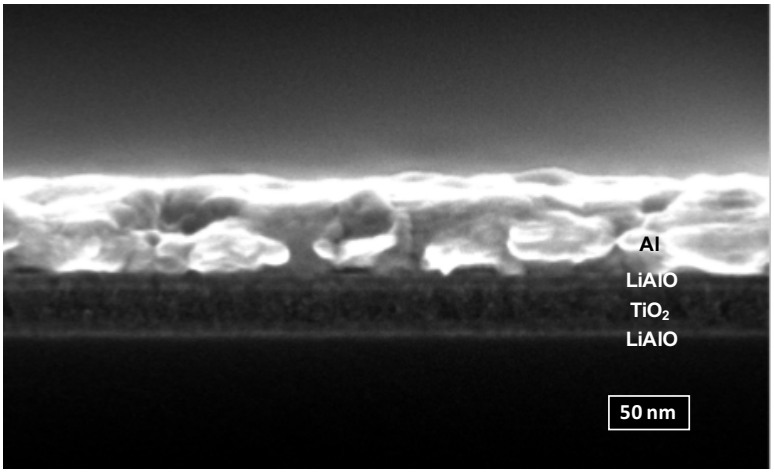

Figure 4.10. Cross-sectional SEM of the thick TiO_2:LiAlO three-layer stack deposited on silicon and annealed at 400 ^oC for one hour.

Electrical characterization of nanolaminate stacks was carried out using impedance spectroscopy. Samples were analyzed at 100 ^oC to promote measurable conduction of Li^+ ions in the LiAlO layers. As previously reported (Chapters II and III), extraction of DC conductivities is challenging and model dependant for thin-film metal-oxide ionic conductors described herein.[83,84,103] Briefly, the real part of the apparent conductivity, σ'_{app}, as a function of frequency yields a small plateau region where the DC

ionic conductivity can be determined. As the electrodes are blocking to conductive ions, polarization at the electrode-film interface manifests as capacitive behaviour at low frequency. At intermediate frequencies a plateau exists that is attributed to the bulk resistance of the electrolyte film. It is at these frequencies where we can estimate film conductivity. The specific frequency of interest corresponds to the peak in the dielectric loss. The conductivity corresponding to this frequency can then be used as an estimate of the DC ionic conductivity. Despite these difficulties, calculated ionic conductivity values are consistent with that of single layer films of comparable thickness (40 nm) and are on the order of 10^{-8} S cm^{-1}. It is somewhat surprising to observe the same conductivities values as pure LiAlO as the introduction of non-conductive TiO_2 is expected to alter the conduction behaviour of the lithium ions. Average DC conductivities among varying nanolaminates are also in good agreement with each other (see Figure 4.11).

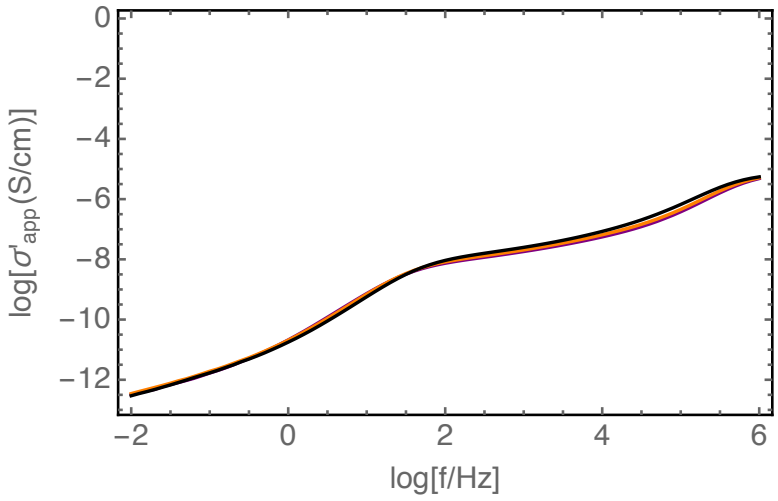

Figure 4.11. The real part of apparent conductivity σ'_{app} as a function of frequency measured at 100 °C of three-layer nanolaminate stacks. Thin TiO_2 (orange line), medium TiO_2 (purple line), and thick TiO_2 (black line).

When capacitance is plotted as a function of frequency, the three types of nanolaminates nearly overlay one another (see Figure 4.12). Low frequency capacitance values, which are independent of thickness, are analogous to single layer films of LiAlO (> 6 μF cm^{-2}). As previously noted, ion polarization against ion blocking electrodes generates an electric double layer that manifests as large increases in the observed capacitance of alkali metal incorporated aluminum oxide.[7,85,87,110,111]

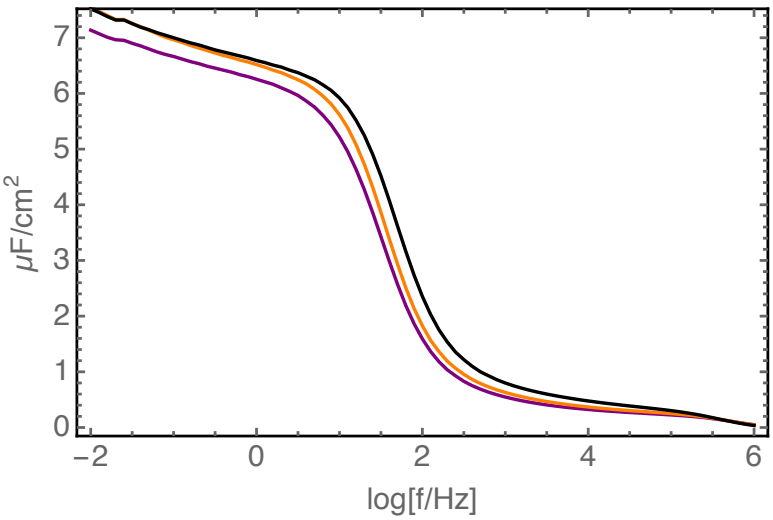

Figure 4.12. Capacitance as a function of frequency of three-layer nanolaminate stacks measured at 100 °C. Thin TiO_2 (orange line), medium TiO_2 (purple line), and thick TiO_2 (black line).

This large capacitance has been primarily cited as a means to lower operating voltages in solid-electrolyte gated field-effect transistors.[7,85] An additional parameter of interest is the amount of energy that can be stored in a dielectric device. The relationship between capacitance and stored energy is defined by the following equation: $W_{stored} = \frac{1}{2}CV^2$ where W is the energy; C is the capacitance; and V is the voltage. The large magnitude of capacitance observed in LiAlO single layer films and nanolaminate stacks

with constituent LiAlO layers is of interest for maximizing stored energy, W. While increasing capacitance is a meaningful goal, a large impact on maximizing the stored energy could also be attained through the increase of the voltage parameter. This voltage parameter is more specifically defined as the maximum voltage that can be applied prior to dielectric failure or breakdown, aptly referred to as the voltage breakdown, V_B. This specific point can be determined by measuring the current as a function of voltage for a particular device. The V_B is identified herein as a rapid increase in the magnitude of current when plotted against the applied voltage (see Figure 4.13). More specifically, the point at which the current rises beyond the noise, defined here as approximately 1 $\mu A\ cm^{-2}$, is assigned as the V_B. When compared to single layer LiAlO films, nanolaminate structures with adequate thicknesses of ion blocking TiO_2 layers exhibit a two-fold increase in the measured V_B, while retaining nearly identical capacitance values (see Figure 4.13). This increase in the observed V_B is in addition to the large capacitance values associated with constituent layers of ion conducting LiAlO observed herein and in single layer LiAlO films (Chapter III). The 7 nm layer of TiO_2 is thought to be too thin to effectively block lithium ions and the breakdown voltage of these nanolaminates are more representative of a single phase LiAlO layers. However, those nanolaminates with TiO_2 layers greater than 10 nm exhibit the substantial increases in measured breakdown strength cited above. This result indicates that nanolaminate structures have a measurable increase in energy storage potential and serve as a valuable means in which to tune material parameters.

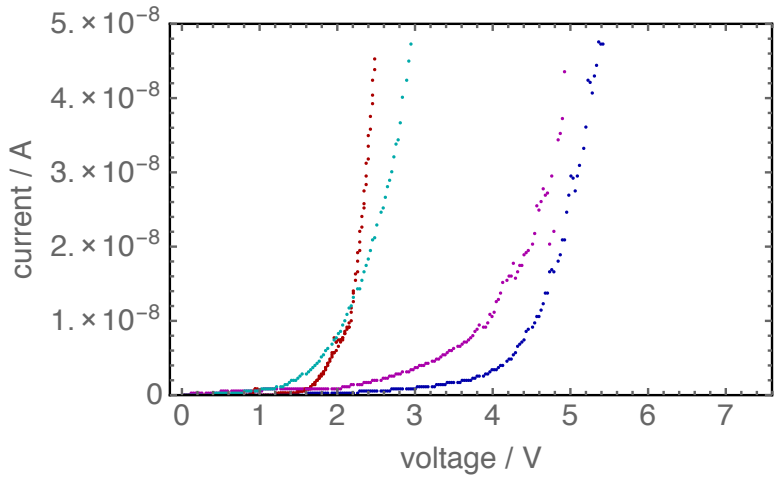

Figure 4.13. Breakdown voltage of LiAlO (red), thin TiO_2:LiAlO nanolaminate (cyan), medium TiO_2:LiAlO nanolaminate (blue), and thick TiO_2:LiAlO nanolaminate (magenta) measured at 100 °C with all thin-film samples annealed at 400 °C for one hour and approximately 40 nm thick.

The observed electrical characteristics are not fully explained by a simple structural model. More specifically, the nanolaminates exhibit properties representative of both single layer and multi-layer films. At low frequency, the observed capacitance is due to the charging of the ionic double layer generated at the electrode-electrolyte interface and is defined by a thickness independent material parameter known as the Debye length. The length of the double layer is the Debye length of the electrolyte, not the thickness of the film. The polarization necessary to form this double layer manifests as a constant contribution to the capacitance, independent of film thickness. This interfacial charging is due to the charging of lithium ions in the LiAlO layers. If the TiO_2 layers are blocking to lithium ions, the system could best be modelled as a series of capacitors, with the total capacitance, C_{total}, represented by the following equation: $C_{total} = \frac{1}{\frac{1}{C_1}+\frac{1}{C_2}+\cdots\frac{1}{C_n}}$. For a layered system with blocking TiO_2, the capacitance should decrease with increasing value of n, where n is the number of layers. The observed low

frequency capacitances of the three types of nanolaminates demonstrate no significant reduction in value and are more consistent with that of single layer films of LiAlO. A possible explanation for the capacitance of the nanolaminates being similar to that of LiAlO films is the ability of lithium to electrochemically insert into TiO_2 (anatase). This would provide a mechanism for additional charge storage. However, the incorporation and conduction of lithium in TiO_2 requires voltages well beyond the 100 mV used to perturb the system during capacitance measurements.[119]

One of the key motivations for the different structures of nanolaminates used in this study was to ensure film abnormalities did not result in areas of layer intermixing. As previously discussed, there is a high level of layer integrity as observed via SEM, with no clear areas of layer mixing. This is especially obvious in nanolaminates that use TiO_2 layers in excess of 25 nm, which have the same capacitance response as those nanolaminates using thinner TiO_2 layers. The governing properties determining the observed behaviours are likely more complex than a series of capacitors or a simple amorphous ionic conducting layer. This is especially true when considering the frequency and temperature dependence of ion motion, which can occur on different timescales resulting in complex representations of the electrical data.

Although strong conclusions regarding the nanostructure of the laminates cannot be ascertained from the capacitance data, the fact that the capacitance remains constant across multiple laminate structures is very interesting. Additionally, the substantial increase in the V_B of the layered stacks is an attractive result. This is especially true when considering the impact this increase in V_B has on the maximum energy storage capacity of the device. Furthermore, the capacitance value is quite large with respect to similar

dielectric films lacking lithium ion incorporation. Collectively, a large capacitance and increase in the breakdown voltage suggest that nanolaminate materials deposited via PIC chemistries are of particular interest with respect to the creation of new structures with interesting material properties.

Conclusion

We have reported the successful synthesis of multi-layered thin films composed of the glassy ionic conductor Li_2O-Al_2O_3 and non-conductive TiO_2 produced via environmentally friendly PIC. Constituent film layers appear smooth, dense, and free of major voids or cracking. A high level of layer integrity is observed among the various nanolaminate structures, suggestive of quality layer interfaces. TiO_2: LiAlO nanolaminate stacks appear amorphous when annealed at 400 °C for one hour. Longer annealing times yield diffraction peaks consistent with anatase TiO_2 thin films produced via PIC.[73] Large capacitance values indicative of an electric double layer were observed in nanolaminate structures as previously reported for ion incorporated alumina.[85] A nearly two-fold increase in voltage breakdown strength is observed in nanolaminate structures over their single phase Li_2O-Al_2O_3 counterparts. This result is significant when considering the effect an increase in V_B has on the amount of energy that can be stored on a device.

CHAPTER V

CONCLUDING SUMMARY

In conclusion, this work has demonstrated the successful use of PIC chemistry for the fabrication of high quality thin film ionic conductors and multi-layered nanolaminates from aqueous solution. Chapter II detailed the first reported synthesis of the ionic conductor LiAlPO in thin-film form. This was also the first time PIC chemistries have been used for the production of solid-state electrolytes. In Chapter III these synthetic methods were expanded to include the inorganic solid-state electrolyte LiAlO, a material more favourable for incorporation into more complex systems. Chapters II and III together, demonstrate that low-cost, environmentally benign synthetic methods can be utilized to produce solid-state conductors with conductivities and activation energies consistent with bulk materials of nominally the same composition but produced via energy intensive processes. Chapter IV focused on the incorporation of LiAlO thin-films detailed in Chapter III into a multi-layered nanolaminate structure. This study extended PIC chemistries beyond the synthesis of multi-layered metal oxides to include structures with ionically conductive constituent layers.

The work presented in this dissertation provides a general description of aqueous solution processing of solid-state electrolytes. This description includes precursor solution properties, film evolution and formation, and electrical performance of resultant films. A deeper understanding of precursor solution chemistries and the associated limitations of these solutions for the deposition of quality thin films is useful beyond this work. Specifically, the controlled concentration of spin coated films and the variables that

govern this process are of interest to any solution processing methods that require the removal of solvents and/or non-target species. Further, an understanding of the variables that impact the chemical interaction and interface quality of multi-layered systems is useful for not only nanolaminates but other energy storage systems including batteries and thin film transistors. Finally, this work serves as a useful step for the continued development of low cost, environmentally sustainable processing of materials important for energy storage.

APPENDIX A

CHAPTER II SUPPLEMENTARY INFORMATION

Portions of this chapter were previously submitted to publish as Clayton, D.C.; Lepage, D.; Plassmeyer, P.N.; Page, C.J.; Lonergan, M.C. Low-Temperature Fabrication of Lithium Aluminum Oxide Phosphate Solid Electrolyte Thin Films from Aqueous Precursors. The excerpt to be included was written entirely by me. D. Lepage, P.N. Plassmeyer, C.J. Page and M.C. Lonergan provided editorial assistance.

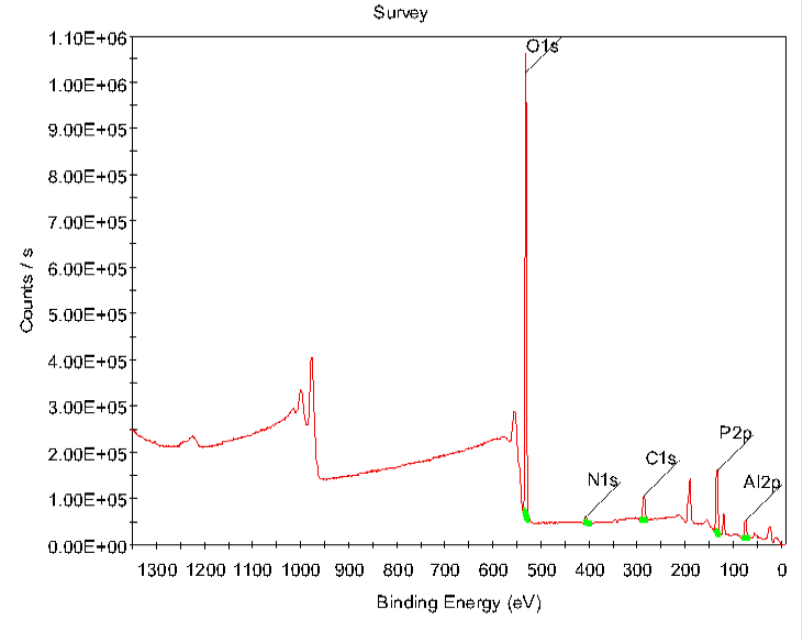

Figure AA1: XPS survey scan of LiAlPO films annealed at 275 °C.

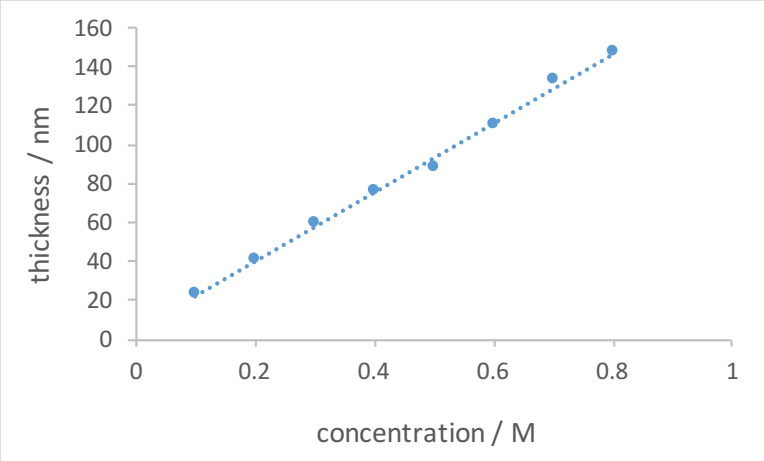

Figure AA2: Thickness as a function of precursor concentration for LiAlPO films resulting from spin-coating precursor solutions at 3000 rpm for 30 s followed by annealing at 275 °C, as determined by x-ray reflectivity and confirmed via ellipsometry.

Table AA1: Atomic ratios of LiAlPO films annealed at 275 °C by XPS

Peak	Atomic Ratio
Al 2p	1
Li 1s	2.5
N 1s	0.1
P 2p	1.6
O 1s	5.8

REFERENCES CITED

1 E. Quartarone and P. Mustarelli, *Chem. Soc. Rev.*, 2011, **40**, 2525-2540.

2 J. Zosel, F. De Blauwe and U. Guth, *Advanced Engineering* , 2001, **3**, 797-801.

3 J. A. Kilner and M. Burriel, *Annu. Rev. Mater. Res.*, 2014, **44**, 365–393.

4 J. B. Goodenough and P. Singh, *J. Electrochem. Soc.*, 2015, **162**, A2387–A2392.

5 C. Zhong, Y. Deng, W. Hu, J. Qiao, L. Zhang and J. Zhang, *Chem. Soc. Rev.*, 2015, **44**, 7484–7539.

6 J. Jensen and F. C. Krebs, *Adv. Mater.*, 2014, **26**, 7231–7234.

7 B. N. Pal, B. M. Dhar, K. C. See and H. E. Katz, *Nature Materials*, 2009, **8**, 898–903.

8 C. Cao, Z. B. Li, X. L. Wang and X. B. Zhao, *Frontiers in Energy Research*, 2014, **2**, 947.

9 J. C. Bachman, S. Muy, A. Grimaud, H.-H. Chang, N. Pour, S. F. Lux, O. Paschos, F. Maglia, S. Lupart, P. Lamp, L. Giordano and Y. Shao-Horn, *Chem. Rev.*, 2016, **116**, 140–162.

10 A. M. Glass and K. Nassau, *J. Appl. Phys.*, 1980, **51**, 3756–3761.

11 R. Tärneberg and A. Lund, *Solid State Ionics*, 1996, **90**, 209–220.

12 J. T. Kummer, *Prog. Solid State Chem.*, 1972, **7**, 141–175.

13 J. B. Goodenough, *Annu. Rev. Mater. Res.*, 2003, **33**, 91–128.

14 K. Funke, *Science and Technology of Advanced Materials*, 2016, **14**, 043502.

15 J. M. Tarascon and M. Armand, *Nature*, 2001, **414**, 359-367.

16 J. B. Goodenough and Y. Kim, *Chem. Mater.*, 2010, **22**, 587–603.

17 P. Knauth, *Solid State Ionics*, 2009, **180**, 911–916.

18 B. B. Owens, *J.Power Sources*, 2000, **90**, 2-8.

19 M. Tatsumisago, M. Nagao and A. Hayashi, *Integrative Medicine Research*, 2013, **1**, 17–25.

20 X.B. Zhao and W.Q. Han, *Frontiers in Energy Research*, 2014, **2**, 1–10.

21 Y. Wang, W. D. Richards, S. P. Ong, L. J. Miara, J. C. Kim, Y. Mo and G. Ceder, *Nature Materials*, 2015, **14**, 1026–1031.

22 N. Kamaya, K. Homma, Y. Yamakawa, M. Hirayama, R. Kanno, M. Yonemura, T. Kamiyama, Y. Kato, S. Hama, K. Kawamoto and A. Mitsui, *Nature Materials*, 2011, **10**, 682–686.

23 H. Aono, *J. Electrochem. Soc.*, 1990, **137**, 1023.

24 A. Dumon, M. Huang, Y. Shen and C.-W. Nan, *Solid State Ionics*, 2013, **243**, 36–41.

25 S. Stramare, V. Thangadurai and W. Weppner, *Chem. Mater.*, 2003, **15**, 3974–3990.

26 R. Kanno and M. Murayama, *J. Electrochem. Soc.*, 2001, **148**, A742.

27 J. L. Souquet, *Ann. Rev. Mater. Sci.*, 1981. **11**, 211-231.

28 A. M. Glass and K. Nassau, *J. Appl. Phys.*, 1980, **51**, 3756–3761.

29 I. D. Raistrick, C. Ho and R. A. Huggins, *Mater. Res. Bull.*, **11**, 953–957.

30 A. M. Glass, K. Nassau and T. J. Negran, *J. Appl. Phys.*, 1978, **49**, 4808–4811.

31 M. Tatsumisago, *Solid State Ionics*, 2004, **175**, 13–18.

32 J. Saienga and S. W. Martin, *J.Non-Cryst. Solids*, 2008, **354**, 1475–1486.

33 X. Yu, J. B. Bates, J. G E Jellison and F. X. Hart, *J. Electrochem. Soc.*, 1997, **144**, 524–532.

34 R. S. Gordon, *Preparation of Solid State Electrolytes, in Inorganic Reactions and Methods: Formation of Ceramics*, John Wiley & Sons, Inc., Hoboken, NJ, USA, 1999, vol. 18.

35 D. M. Mattox, *Metal Finishing*, 2001, **99**, 409–423.

36 M. Ritala and M. Leskelä, *Thin Solid Films*, 2002, **409**, 138-146.

37 A. E. Danks, S. R. Hall and Z. Schnepp, *Materials Horizons*, 2016, **3**, 91–112.

38 C. J. Brinker and G. W. Scherer, *Sol-Gel Science: The Physics and Chemistry of Sol-Gel Processing*, Academic Press, Inc., San Diego, CA, USA, 2013.

39 Y. Aoki, T. Kunitake and A. Nakao, *Chem. Mater.*, 2005, **17**, 450–458.

40 M. Bockmeyer and P. Löbmann, *Thin Solid Films*, 2007, **515**, 5212–5219.

41 K. Kajihara, *Integrative Medicine Research*, 2013, **1**, 121–133.

42 S. T. Meyers, J. T. Anderson, D. Hong, C. M. Hung, J. F. Wager and D. A. Keszler, *Chem. Mater.*, 2007, **19**, 4023–4029.

43 K. M. Norelli, P. N. Plassmeyer, K. N. Woods, B. A. Glassy, C. C. Knutson, M. Beekman and C. J. Page, *Solid State Sciences*, 2016, **55**, 8–12.

44 W. Wang, K. M. Wentz, S. E. Hayes, D. W. Johnson and D. A. Keszler, *Inorg. Chem.*, 2011, **50**, 4683–4685.

45 J. T. Anderson, W. Wang, K. Jiang, T. Gustafsson, C. Xu, E. L. Gafunkel and D. A. Keszler, *ACS Sustainable Chem. Eng.*, 2015, **3**, 1081–1085.

46 M. Alemayehu, J. E. Davis, M. Jackson, B. Lessig, L. Smith, J. D. Sumega, C. Knutson, M. Beekman, D. C. Johnson and D. A. Keszler, *Solid State Sciences*, 2011, **13**, 2037–2040.

47 D. A. Keszler, J. T. Anderson and S. T. Meyers, in *Solution Processing of Inorganic Materials*, John Wiley & Sons, Inc., 2008, pp. 109–129.

48 A. J. Sillanpää, J. T. Päivärinta, M. J. Hotokka, J. B. Rosenholm and K. E. Laasonen, *J. Phys. Chem. A*, 2001, **105**, 10111–10122.

49 E. C. de Oliveira Lima, J.M. Moita Neto, F.Y. Fujiwara and F. Galembeck, *J. Colloid Interface Sci.*, 1996, **176**, 388-396.

50 K. Jiang, J. T. Anderson, K. Hoshino, D. Li, J. F. Wager and D. A. Keszler, *Chem. Mater.*, 2011, **23**, 945–952.

51 P. N. Plassmeyer, G. Mitchson, K. N. Woods, D. C. Johnson and C. J. Page, *Chem. Mater.*, 2017, **29**, 2921–2926.

52 S. T. Meyers, J. T. Anderson, C. M. Hung, J. Thompson, J. F. Wager and D. A. Keszler, *J. Am. Chem. Soc.*, 2008, **130**, 17603–17609.

53 J. Azadmanjiri, C. C. Berndt, J. Wang, A. Kapoor, V. K. Srivastava and C. Wen, *J. Mater. Chem. A*, 2014, **2**, 3695.

54 M. Osada and T. Sasaki, *Adv. Mater.*, 2011, **24**, 210–228.

55 Y. Aoki and T. Kunitake, *Adv. Mater.*, 2004, **16**, 118–123.

56 W. J. Zhu, T. Tamagawa, M. Gibson, T. Furukawa and T. P. Ma, *IEEE Electron Device Lett.*, 2001, **23**, 649–651.

57 M. H. Cho, Y. S. Roh, C. N. Whang, K. Jeong, H. J. Choi, S. W. Nam, D. H. Ko, J. H. Lee, N. I. Lee and K. Fujihara, *Appl. Phys. Lett.*, 2002, **81**, 1071–1073.

58 S. Lee and D.-L. Kwong, *Jpn. J. Appl. Phys.*, 2004, **43**, 427–431.

59 H. S. Chang, S. Jeon, H. Hwang and D. W. Moon, *Appl. Phys. Lett.*, 2002, **80**, 3385–3387.

60 P. K. Park, E.-S. Cha and S.-W. Kang, *Appl. Phys. Lett.*, 2007, **90**, 232906–4.

61 W. Li, Z. Chen, R. N. Premnath, B. Kabius and O. Auciello, *J. Appl. Phys.*, 2011, **110**, 024106–9.

62 E. Miranda, J. Suñé, T. Das, C. Mahata and C. K. Maiti, *J. Appl. Phys.*, 2012, **112**, 064113–9.

63 I. J gi, K. Kukli, M. Kemell, M. Ritala and M. Leskel, *J. Appl. Phys.*, 2007, **102**, 114114–12.

64 J. W. Elam, Z. A. Sechrist and S. M. George, *Thin Solid Films*, 2002, **414**, 43–55.

65 J. M. Jensen, A. B. Oelkers, R. Toivola, D. C. Johnson, J. W. Elam and S. M. George, *Chem. Mater.*, 2002, **14**, 2276–2282.

66 Y. Cao, P. C. Irwin and K. Younsi, *IEEE Transactions on Dielectrics and Electrical Insulation*, 2004, **11**, 797–807.

67 P. Kim, X. H. Zhang, B. Domercq, S. C. Jones, P. J. Hotchkiss, S. R. Marder, B. Kippelen and J. W. Perry, *Appl. Phys. Lett.*, 2008, **93**, 013302–4.

68 W. Li, O. Auciello, R. N. Premnath and B. Kabius, *Appl. Phys. Lett.*, 2010, **96**, 162907–4.

69 P. Barber, H. Houghton, S. Balasubramanian, Y. K. Anguchamy, H. J. Ploehn and H. C. zur Loye, *Chem. Mater.*, 2009, **21**, 1303–1310.

70 S. P. Fillery, H. Koerner, L. Drummy, E. Dunkerley, M. F. Durstock, D. F. Schmidt and R. A. Vaia, *ACS Appl. Mater. Interfaces*, 2012, **4**, 1388–1396.

71 J. T. Anderson, C. L. Munsee, C. M. Hung, T. M. Phung, G. S. Herman, D. C. Johnson, J. F. Wager and D. A. Keszler, *Adv. Funct. Mater.*, 2007, **17**, 2117–2124.

72 K. Takada, *Acta Materialia*, 2013, **61**, 759–770.

73 K. Jiang, A. Zakutayev, J. Stowers, M. D. Anderson, J. Tate, D. H. McIntyre, D. C. Johnson and D. A. Keszler, *Solid State Sciences*, 2009, **11**, 1692–1699.

74 K. Jiang, S. T. Meyers, M. D. Anderson, D. C. Johnson and D. A. Keszler, *Chem. Mater.*, 2013, **25**, 210-214.

75 M. V. N. V. D. Sharma, A. V. Sarma and R. Balaji Rao, *J Mater Sci*, 2009, **44**, 5557–5562.

76 Y. Wang, Z. Liu, X. Zhu, Y. Tang and F. Huang, *J. Power Sources*, 2013, **224**, 225–229.

77 M. S. Bhuiyan and M. Paranthaman, *Science and technology*, 2006, **19**, R1-R21.

78 Y. Aoki, T. Kunitake and A. Nakao, *Chem. Mater.*, 2005, **17**, 450–458.

79 E. J. van den Ham, N. Peys, C. De Dobbelaere, J. D'Haen, F. Mattelaer, C. Detavernier, P. H. L. Notten, A. Hardy and M. K. Van Bael, *J Sol-Gel Sci Technol*, 2014, **73**, 536–543.

80 S. Yuvaraj, L. Fan-Yuan, C. Tsong-Huei and Y. Chuin-Tih, *J. Phys. Chem. B*, 2003, **107**, 1044–1047.

81 C. V. Koti Reddy, R. Balaji Rao, K. Chandra Mouli, D. V. Rama Koti Reddy and M. V. Ramana Reddy, *J Mater Sci*, 2012, **47**, 6254–6262.

82 W. Xu, H. Wang, F. Xie, J. Chen, H. Cao and J.-B. Xu, *ACS Appl. Mater. Interfaces*, 2015, **7**, 5803–5810.

83 J. R. Macdonald, *Phys. Rev. B*, 2005, **71**, 184307.

84 F. Lin, Y. Wang and M. Lonergan, *J. Appl. Phys.*, 2008, **104**, 103517.

85 Y. Liu, P. Guan, B. Zhang, M. L. Falk and H. E. Katz, *Chem. Mater.*, 2013, 130918064757004.

86 J. Sun, C. Qian, W. Huang, J. Yang and Y. Gao, *Phys. Chem. Chem. Phys.*, 2014, **16**, 7455.

87 Y. Liu, A. K. Diallo and H. E. Katz, *Appl. Phys. Lett.*, 2015, **106**, 112906.

88 B. Wang, J. Liu, Q. Sun, R. Li, T.-K. Sham and X. Sun, *Nanotechnology*, 2015, **25**, 1–8.

89 I. A. Sokolov, Y. P. Tarlakov, N. Y. Ustinov and A. A. Pronkin, *Russ. J. Appl. Chem.*, 2005, **78**, 741–746.

90 I. Jlassi, H. Elhouichet and M. Ferid, *Physica E*, 2016, **81**, 219–225.

91 S. Duluard, A. Paillassa, L. Puech, P. Vinatier, V. Turq, P. Rozier, P. Lenormand, P.-L. Taberna, P. Simon and F. Ansart, *J. Eur. Ceram. Soc.*, 2013, **33**, 1145–1153.

92 B. Key, D. J. Schroeder, B. J. Ingram and J. T. Vaughey, *Chem. Mater.*, 2012, **24**, 287–293.

93 J. K. Feng, L. Lu and M. O. Lai, *J. Alloys Compd.*, 2010, **501**, 255–258.

94 J. F. M. Oudenhoven, L. C. Baggetto and P. H. L. Notten, *Adv. Energy Mater.*, 2010, **1**, 10–33.

95 K. Kinoshita, J. W. Sim and J. P. Ackerman, *Mater. Res. Bull.*, 1978, **13**, 445–455.

96 R. N. Singh, J. T. Dusek and J. W. Sim, *Am. Ceram. Soc. Bull.;(United States)*, 1981, **60**, 629-635.

97 F. Oksuzomer, S. N. Koc, I. Boz and M. A. Gurkaynak, *Mater. Res. Bull.*, 2004, **39**, 715–724.

98 F. Li, K. Hu, J. Li, D. Zhang and G. Chen, *J. Nucl. Mater.*, 2002, **300**, 82–88.

99 E. Caudron, G. Baud, J. P. Besse, M. Jacquet and G. Blondiaux, *Solid State Ionics*, 1994, **70–71**, 629–635.

100 T. Aaltonen, O. Nilsen, A. Magrasó and H. Fjellvåg, *Chem. Mater.*, 2011, **23**, 4669–4675.

101 D. J. Comstock and J. W. Elam, *J. Phys. Chem. C*, 2013, **117**, 1677–1683.

102 A. Nadarajah, M. Z. B. Wu, K. Archila, M. G. Kast, A. M. Smith, T. H. Chiang, D. A. Keszler, J. F. Wager and S. W. Boettcher, *Chem. Mater.*, 2015, **27**, 5587–5596.

103 D. R. Clayton, D. Lepage, P. N. Plassmeyer, C. J. Page and M. C. Lonergan, *RSC Advances*, 2017, **7**, 7046–7051.

104 G. D. Robertson Jr and D. M. Mason, *J.Phys. Chem.*, 1955, **59**, 683–690.

105 H. Qin, P. Sutter and G. Zhou, *J Am. Ceram. Soc.*, 2014, **97**, 2762–2769.

106 L. H. Jones, *J. Chem. Phys.*, 1954, **22**, 217–219.

107 I. Gennick and K. M. Harmon, *Inorg. Chem.*, 1975, **14**, 2214–2219.

108 J. M. Saniger, *Mater. Lett.*, 1995, **22**, 109–113.

109 Z. Qing, B. Li, H. Li, Y. Li and S. Zhang, *J Mater Sci: Mater Electron*, 2014, **25**, 2149–2154.

110 J. Kruempelmann, C. R. Mariappan, C. Schober and B. Roling, *Phys. Rev. B*, 2010, **82**, 38–6.

111 C. R. Mariappan, T. P. Heins and B. Roling, *Solid State Ionics*, 2010, **181**, 859–863.

112 G. D. Wilk, R. M. Wallace and J. M. Anthony, *J. Appl. Phys.*, 2001, **89**, 5243.

113 A. Roy Chaudhuri, A. Fissel, V. R. Archakam and H. J. Osten, *Appl. Phys. Lett.*, 2013, **102**, 022904–5.

114 B. Roling, C. Martiny and S. Brückner, *Phys. Rev. B*, 2001, **63**, 214203.

115 L. G. Parratt, *Physical Review*, 1954, **95**, 359–369.

116 D. R. Merrill, D. B. Moore, J. Ditto, D. R. Sutherland, M. Falmbigl, M. Winkler, H.-F. Pernau and D. C. Johnson, *Eur. J. Inorg. Chem.*, 2014, **2015**, 83–91.

117 K. C. Fairley, D. R. Merrill, K. N. Woods, J. Ditto, C. Xu, R. P. Oleksak, T. Gustafsson, D. W. Johnson, E. L. Garfunkel, G. S. Herman, D. C. Johnson and C. J. Page, *ACS Appl. Mater. Interfaces*, 2016, **8**, 667–672.

118 D. R. G. Mitchell, D. J. Attard, K. S. Finnie, G. Triani, C. J. Barbé, C. Depagne and J. R. Bartlett, *Appl. Surf. Sci.*, 2005, **243**, 265–277.

119 K. H. Reiman, K. M. Brace, T. J. Gordon-Smith, I. Nandhakumar, G. S. Attard and J. R. Owen, *Electrochem. Commun.*, 2006, **8**, 517–522.